

# CHAPTER 1

## Introduction

Helium-cooled pebble beds (HCPB) of lithium ceramics exist in candidate designs of tritium breeding devices of many current nuclear fusion demonstration reactor designs as well as tritium breeding modules to be tested in the ITER experiment. HCPBs will be used to generate high quality heat for electricity production and breed tritium for a self-sustained fuel cycle. Pebble bed forms of tritium breeding volumes have several advantages which include: ease of assembly of granular materials into complex geometries; bred tritium can be readily removed via a helium purge gas through interstitial porous networks; temperature gradients across any single pebble are small enough to avoid damage from thermal stress.

A relatively narrow operational temperature window for optimum breeding performance of ceramics must be observed to respect temperature-dependent phenomena driving tritium release from lithiated ceramic pebbles. It is therefore necessary to have accurate knowledge of ceramic pebble bed thermomechanical behavior and comprehensive characterization; reliable models of heat transfer in solid breeders are critical for solid breeder designs. However, temperature prediction in ceramic pebble beds remains a challenge for many reasons. After packing the ceramic pebbles into a containment structure, there exists a coupling between mechanical forces acting upon beds and their heat transport capabilities. In addition, some amount of restructuring of the pebble bed and the internal contact force network is likely to occur in HCPBs from crushing/cracking of individual pebbles, inter-pebble sintering, or creep during operation. Contact conduction in beds, intimately linked to the packing structure, will subsequently be impacted during operation of ceramic pebble beds in fusion reactors. Concurrently, interaction of the slow-moving purge gas with tightly packed pebble beds is an additional route of heat transfer that must be understood. Thus, heat transfer in pebble

beds is quite different from standard solid materials and requires specialized modeling of the synergistic physics. Knowledge and characterization of thermal transport must anticipate changes to the heat transfer capabilities and predict temperature profiles for pebble bed packing structures that will emerge after initially-packed pebble beds react to prolonged exposure to fusion reactor environments.

In the remaining sections of this chapter I will present more background on the role of ceramic pebble beds in tokamak fusion reactors, more thorough descriptions of solid breeder blanket designs, and the objectives of this study.

## 1.1 Description of Ceramic Pebble Bed Designs for Tritium Breeding

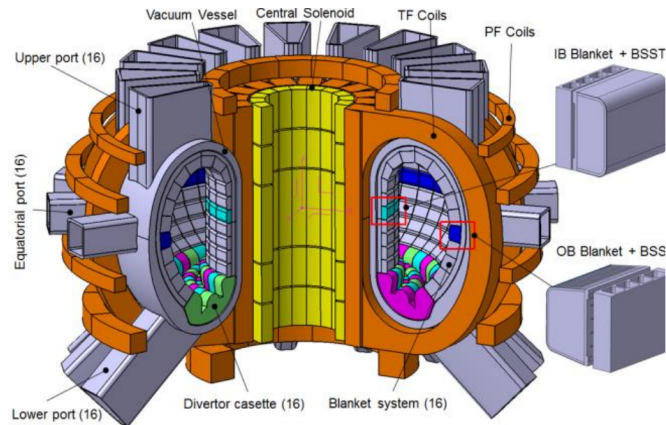


Figure 1.1: An example design of a DEMO reactor with solid breeder blankets shown as inboard (IB) and outboard (OB) blanket components.

The fusion reactor as a promising energy supplier has been intensively studied for decades. The economic, safety, and environmental attractiveness of fusion reactors will be determined, to a large extent, by the choice of materials for the performance of the blanket. Specifically, for a solid breeder blanket concept, issues such as the thermomechanics of solid breeder materials and irradiation effects on tritium release characteristics remain to be addressed in more detail.

The successful operation of a breeder unit will see the device capture neutrons ejected from the fusion reaction to generate fuel for self-sufficiency via the transmutation of lithium into tritium, act as shield to other sensitive equipment and personnel, and convert energy into extractable heat for electricity production. Figure 1.1 shows an example sketch of a demonstration (DEMO) fusion reactor and the relative location of the breeder blanket modules as they will face the plasma in the torus of the tokamak.

Since the inception of the solid breeder concept in the late 1970s, designs have evolved in response to operational requirements of harsh fusion reactor environments. Currently, the reference solid breeder design incorporates packed beds of ceramic pebbles (spherical particles) that are filled into containment structures. In a typical solid breeder module, the breeding volume is subdivided into several alternating layers of neutron multiplication material (generally beryllium) and tritium breeding material. The layers are separated by coolant plates with internal channels for coolant. The coolant is typically a high pressure helium though some designs call for pressurized water, in spite of the dangers of the highly exothermic reaction with oxygen from water vapor and lithium in the case of coolant leak. After a neutron strikes lithium for the creation of tritium, the bred hydrogen isotope diffuses through the ceramic material until being picked up by a low-pressure, slow moving purge gas (primarily helium) and extracted in a closed loop for fuel.

## 1.2 Solid Breeder Thermal Management and Imposed Temperature Window

To understand the importance of predictive capabilities of temperature in solid breeders, we first consider one of the main roles of the breeder is to readily allow tritium to be extracted. Therefore we can first consider the path of tritium from its generation until it is swept away by the helium purge gas; the journey of tritium is shown schematically in Figure 1.2. Tritium begins its life internally inside pebbles. Tritium then diffuses slowly through the bulk of the ceramic lattice until reaching a grain boundary. At this point, tritium diffuses more quickly along the grain boundary until reaching a surface of open porosity where it may desorb into

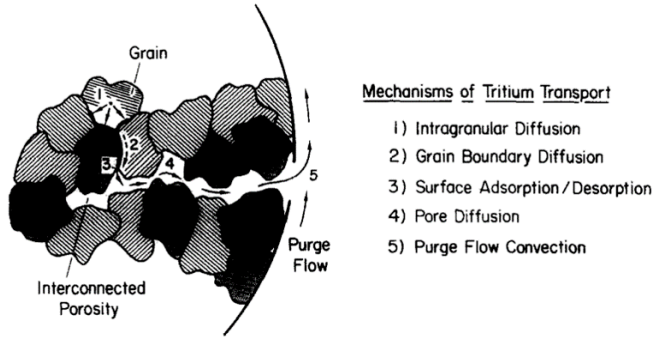


Figure 1.2: Mechanisms of tritium transport in a single pebble.<sup>50</sup>

stagnant gas in a pebble's open porosity. Finally, tritium diffuses more rapidly still through the gas until being swept up in the advection of helium purge gas.<sup>50</sup>

Experiments on tritium inventory have attempted to quantify the speeds of tritium release and found that bulk diffusion of tritium, typically the slowest transport mode, is a direct function of temperature.<sup>58</sup> Thus the lower temperature limit,  $T_{\min}$ , of temperature windows for solid breeders, is based on the unacceptable tritium inventory due to slow bulk diffusion. The value of  $T_{\min}$  is generally around 300 °C. Using the same model of tritium transport, bulk diffusion also limits the maximum temperature in the solid breeder temperature window. Exposure to prolonged high temperature environments causes individual grains in a pebble to grow. Grain growth therefore extends the characteristic length of the slowest mode of tritium transport. Thus the maximum temperature,  $T_{\max}$ , of the operational window for ceramic pebble beds is generally placed around 80% of the melt temperature of the ceramic,  $T_{\max} = 0.8T_{\text{melt}}$ , to avoid surface sintering. For many lithium ceramics, this value falls around 900 °C.

As a consequence of the tritium release from the solid breeder material, we are faced with a relatively narrow operational temperature to which solid breeder designers must adhere. Thus to provide designers the ability to optimize breeder volumes for tritium release, we must understand the important physics and phenomena dictating thermomechanical responses of pebble beds during use in a fusion reactor.

Figure 1.3 shows a generic solid breeder volume that is common in current designs of tritium breeding modules for ITER. Tritium breeding blankets will experience high vol-

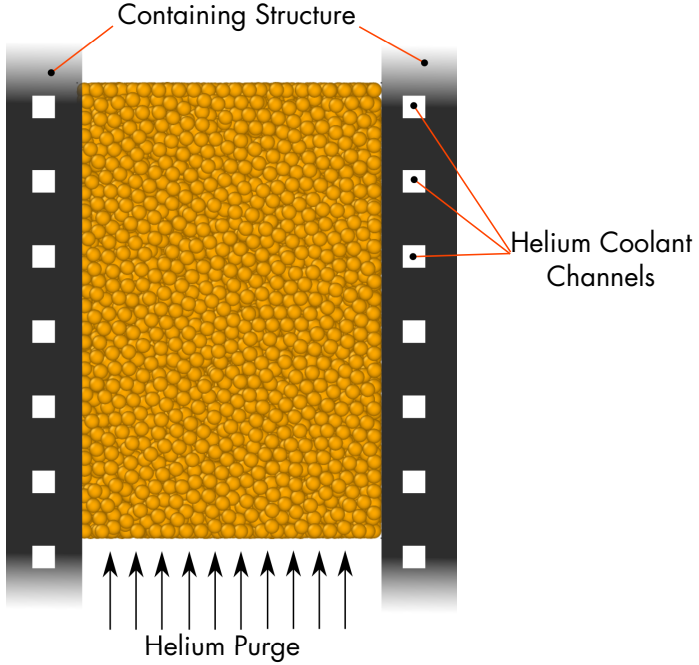


Figure 1.3: Sketch of a typical unit of a pebble bed tritium breeding zone. The pebble bed is cooled with contact to the containing structure.

metric heating as deposited by high-energy neutrons that are carrying away approximately 80% of the fusion reaction energy as well as secondary  $\gamma$  rays. The deposited heat must be transported through the pebble bed region into the walls of the containing structure, then ultimately into the coolant gas. Heat deposited into pebble beds will transfer via inter-particle contact conduction, inter-particle radiation, and convection with the helium purge gas. At the interface with the structural material, similar modes of heat transfer are present: particle-wall contact conduction, particle-wall radiation, and communication via helium purge gas convection. As the pebbles heat under the nuclear load, thermal expansion of the pebbles in the packed volume will be contained by relatively cooler structural material. Confined expansion will give rise to increased contact pressure between pebbles. Pressure on pebble beds is known to be the cause of many phenomena, some of which directly impact the thermal transport characteristics of pebble beds and may ultimately jeopardize the reliable and safe operation of breeding blankets.

The packing structure of packed beds can be considered as a metastable configuration

that will last indefinitely unless acted upon by an external perturbation such as vibration or compressive pressure.<sup>89</sup> The ability of a metastable configuration to resist perturbations can in some way be quantified by the initial packing fraction. For more compliant beds, with lower packing fractions, the stresses from thermal expansion can cause significant rearrangement of the packing structure which is not recoverable after removing the stress. This phenomena has been observed in numerous experiments as so-called plastic rearrangement of pebble beds.<sup>126,127,178</sup> Plasticity of beds may have significant consequences for the ability of the pebble bed to maintain contact with the containing structure and routes for heat out of the bed due to gap formation between the two materials. Moreover, increased pressure between pebbles can cause the brittle pebbles themselves to fragment which will also disrupt paths of heat in the inter-particle conduction network. The consequence of both the mentioned effects is an increase in the temperature of bed pebbles. If the fragments are sufficiently small, they may even cause blockage of the helium purge gas.

Due to the complicated nature of granular materials such as ceramic pebble beds, heat transfer in these solid breeder volumes should not be considered as a static phenomena that can be characterized prior to inserting pebbles beds into breeder modules and then expected to behave consistently after long exposure to fusion environments. Pebble bed temperatures, linked to the packing, will evolve in ways that are currently not predictable and must be studied and modeled.

In spite of their many engineering applications, heat transfer mechanisms in packed beds of granular material are still not thoroughly understood nor characterized. Hence, one approach is to treat the granular material as a fictitious continuous media, an approach adopted by several designers of solid breeders. Many experiments have been carried out for developing phenomenological models for effective material properties. In this approach, heat transport in pebble beds is often characterized with an effective thermal conductivity,  $k_{\text{eff}}$ . Many models have shown their ability to accurately predict the temperature profiles for pebble beds under specific operating conditions. However, the accuracy of the model predictions often degrade as soon as a pebble bed's granular material, grain radii distributions, or operating conditions vary from the experimentally studied packed beds. In addition, propensity for

creep, crushing, and inter-particle sintering of ceramic materials alter the packing structure in ways not currently predictable with the effective material characterizations. Furthermore, effective conductivity models that consider interstitial gas often assume the gas is stagnant. The assumption has not been thoroughly vetted and is likely insufficient to capture the thermal influence of the helium purge gas flowing through the ceramic pebble beds in fusion reactors.

To overcome the limitations of effective material modeling, and aided by the acceleration and availability of computational power, many researchers of granular heat transfer have shifted their attention to studies of the interacting physics on grain-scales. In this approach, we interrogate heat transfer on the scale of particle interactions and model transient, grain-scale behavior in packed beds. We can then couple grain-scale models of heat transfer and mechanics to either volume-averaged fluid models or models of the entire tortuous fluid flow through the porous network of packed beds. note: have to mention that i'm using DEM I guess. maybe in the objectives section?

### 1.3 Objectives of this Study

The goal of this work is to develop more comprehensive and accurate models for predicting temperature distributions in ceramic pebble beds, accounting for many important phenomena including pebble crushing and fragmentation, dynamic analysis of packing restructuring, and considerations of inter-porous helium purge gas. In particular I will study in great detail the relationship between morphological changes to packing structures and the resulting changes to heat transfer in packed beds. In particular, I will be concerned with the nuclear heating of pebble fragments as they redistribute through pebble beds and come to rest without strong mechanical contact (and therefore contact conductance) to neighboring pebbles. This includes analyzing changes to temperature distributions in pebble beds with different models of pebble damage, analyzing the impact of helium flow on temperatures in beds with fragmented pebbles, and changes to bed stresses and contact-force networks in beds with restructured packing. Experimental efforts will inform numerical development at the start.

Following, numerical model development and application and extensive data analysis will be the main approach taken in this study. Satisfying the objectives of this work includes several major efforts that can be summarized as follows:

Experimental campaigns crushing various lithium ceramic pebbles ( $\text{Li}_2\text{TiO}_3$  and  $\text{Li}_4\text{SiO}_4$ ) between two nickel-based steel alloys will be carried out at temperatures ranging from room temperature to  $650^\circ\text{C}$  to observe the temperature-dependence of crush strength. From the experimental data, I will also validate the Hertzian assumption for contact mechanics of the spherical pebbles on the flat pistons; experiments measure the force-travel response of individual pebbles and, via comparison with predictions of Hertz theory, will show a modified Young's modulus is necessary for use in the material inputs. The crush experiments will also be used as a basis for developing a criteria for prediction of pebble crushing in packed beds.

Numeric campaigns will develop in stages. In the first stage, many components of the pebble bed modeling will be tested individually. Simulations strictly of heat transfer dependence on pebble interactions (without consideration of fluid flow) will be executed to analyze the links between pebble descriptions (*e.g.* packing fraction, coordination number, contact forces) and temperature distributions in pebble beds with specific models of pebble damage. A study will apply the modified Young's modulus model to show the dependence of crush predictions and external measured stresses of beds on the Young's modulus assigned to pebbles in simulations. Finally, another separate study will assess the impact of fragment size on packing resettling and its role in thermal transport.

In the second stage, pebble beds similar to the first stage will be analyzed, with and without helium flow. In this stage, the helium flow will be two-way coupled to the pebble bed with fluid phase being characterized with volume-averaged conservation equations. We will see the role of helium on smoothing out temperatures between pebbles which have poor mechanical contact with neighbors in the assembly. Again, effective thermal conductivity measurements will be reported from well-packed beds and beds with pebble damage. Lastly, in this stage, several ITER-relevant configurations of pebble beds are studied.

In the third stage, pebble beds are one-way coupled to models of helium flow. Rather

than considering volume-averaged conservation equations, we will make use of the novel approach of solving lattice-Boltzmann equation on discretized lattice nodes which allow for simple application of boundary conditions on the complex geometry of packed beds. This approach will provide a more complete view of helium's serpentine route through the pebble bed and its impact on temperature distributions in beds.

## 1.4 Dissertation Outline

In the next chapter I will present a literature review on the state of the art of modeling granular materials and packed beds, including: effective thermal conductivity experiments and their derivative empirical relationships, convective energy exchange in packed bed media, and drag of fluid flow through packed beds. The literature review also discusses the specific application of granular research for packed beds in the fusion community, highlighting progress made and where deficiencies in research remain. In ??, I will present the theory behind the discrete element method modeling for granular interaction as well as experimental efforts to validate Hertz theory and aid in development of pebble damage modeling. Then ?? covers the coupling of the pebble model in DEM to the volume-averaged CFD as well as coupling to solvers of the lattice-Boltzmann equation. After model development is complete, in ??, I begin application of the models to study of temperature distributions in ceramic pebble beds for tritium breeding; first models are run only in the DEM environment, then with the coupled CFD-DEM models, and finally with coupled DEM-LBM simulations. Finally in ?? a summary of the work, the impact of the results, and a suggestion for future work will be presented.

# CHAPTER 2

## Literature Review

Ceramic pebble beds in solid breeders can be seen as belonging to a larger class of generalized granular material, and specifically dry granular material. A deceptively simple definition of a granular material is one for which the medium cannot be described in terms of traditional Brownian motion.<sup>46</sup> Granular materials can also be described as a aggregation of discrete, macroscopic particles (mean size greater than 100  $\mu\text{m}$ ) that are characterized with energy dissipation during interaction. The study of ceramic pebble bed thermomechanics for tritium breeding have their roots connected to historical treatment of granular material and it is instructive to begin with a short review of this field. Following that, I will compile many generalized studies of heat and momentum transfer, specifically correlations that have been developed in the classical continuum treatment of pebble beds. The correlations will not only be instructive by view of their limitations, but they will help inform the numerical modeling of coupling fluid and pebble bed conservation equations. Finally, I will focus the literature review specifically on the progress that has been made in temperature predictions from numerical models of tritium breeders for fusionr eactors.

### 2.1 Brief History of Granular Material Research

The science and modeling of granular materials has a long and rich history. Coulomb proposed ideas of static friction in 1773, Faraday in 1831 discovered the convective movement of powders, and even Reynolds in 1885 introduced notions on granular expansion and shear.<sup>90</sup> Yet despite the diverse fields interested in granular materials, the description of them with classic continuum mechanics is still far from complete; quite different from the conclusively

described constitutive equations of elastic theory, hydrodynamics, and gas dynamics that have existed for two centuries.<sup>137</sup> Granular materials are only second to water in terms of most-used industrial material. Granular materials play an important role in civil, geotechnical, chemical, and mechanical engineering in industries as diverse as pharmacy, automotive, agriculture, and construction to name just a few.<sup>46,82</sup> A resurgence of interest in granular materials has also happened in the fields of applied mathematics and physics as metaphors for other dynamical systems.<sup>90</sup>

Even if we restrict our consideration to static packings of non-cohesive granular materials (neglecting the complex, unusual granular hydro- and gas dynamics), modeling is complicated by the heterogeneity of contact forces running through the packed grains and the packing structure of the grains. The granular medium introduces complexity to modeling, in part, due to its significant difference between compression and tension experiments; under compression the granular medium behaves as if an elastic or elasto-plastic body but offers no resistance to tension. Furthermore, when an external excitation, such as vibration, is introduced into the metastable packing state of a granular system, the packing is unlocked to slowly travel through packing phase space at a logarithmically slow pace [Barker and Mehta 1993, Mehta 1994, Knight 1995].

Nonetheless, many material models have been developed in an attempt to describe the mechanics of a granular system as a fictitious continuum with varying success and applicability. Researchers in geophysics have long viewed granular materials as continuous materials for which they painstakingly developed equations as if the granular material obeyed laws of classical mechanics.<sup>46</sup> [cite Drucker and Prager, etc. see<sup>82</sup>]. Heat transfer in granular materials has also been treated in a continuum manner and the correlations will be covered in explicit detail in § 2.2.

Granular system became important to fusion power reactors after the introduction of a solid, non-mobile tritium breeding blanket design concept by Abdou *et al.*<sup>1</sup> in 1975, the so-called ‘solid breeder’ or ‘ceramic breeder’ beds of lithium ceramics. Because of the large size scale and complex interactive physics of solid breeders, it is desirable to employ the continuum-based models on the packed beds of ceramics with effective thermomechanical

properties derived from experiments on granular beds. In § 2.4, the status and success of early continuum-based models will be discussed in more detail.

In 1979, Cundall & Strack opened a new avenue for studying granular materials when they introduced the distinct element method (later renamed by the community as the *discrete* element method).<sup>34</sup> Since then, grain-scale descriptions of granular systems have taken prominence for their ability to enrich the macrosopic models when they are insufficient to describe the rheology of a granular material. In the approach of Cundall & Strack, all of the individual grains in a system are described as rigid elements for which the equations of motion can each be simultaneously integrated based on the (typically localized) interacting forces.

## 2.2 General Studies of Heat Transfer in Granular Material

For packed beds of ceramic spheres filled into tritium breeding modules, we identify the following modes of simultaneous heat transfer:

### 1. Inter-granular conduction

- Conduction through the contact area between contacting particles.
- Conduction through the contact area between particles in contact with structural walls.

### 2. Granular-fluid interaction

- Conduction through the stagnant fluid between near, non-contacting particles.
- Conduction through the stagnant fluid between contacting particles.
- Smoluchowski effect of non-Knudsen fluid conduction in near-granular regions.
- Advection of energy by the fluid to contacting- and downstream particles.

### 3. Radiation effects

- Radiation between the surfaces of contacting particles.

- Radiation between the surfaces of particles through adjacent voids.
- Heat generation internally in the particle from incident neutron fluxes.

Historically, granular materials are treated as a fictitious continuous media for which effective properties or correlations are derived. In this section. The volume of a pebble in a tritium breeder is on the scale of  $10 \times 10^{-9} \text{ m}^3$  while the typical container volume can be on the order of  $10 \times 10^{-2} \text{ m}^3$ .<sup>29</sup> Thus a single breeder volume will house upwards of  $N = 10 \times 10^7$  pebbles. Statistically then, it is reasonable to assume that a ceramic pebble bed can be treated as a fictitious granular material for which continuum theory is applicable. This assumption is the basis of many correlations for heat transfer in granular material. The continuum assumption also underpins application of finite element method (FEM) models for breeder pebble beds; constitutive equations are developed from experimental measurements of the macroscopic behavior of pebble beds which are fed into FEM models.

### 2.2.1 Effective Thermal Conductivity of Granular Media

Deissler and Boegli, in 1958, proposed upper and lower bounds of effective thermal conductivity,  $k_{\text{eff}}$ , in two-phase granular media to be given by alternating layers of the two phases arranged in parallel or series, respectively.<sup>37</sup> In the case of parallel layers, effective conductivity, normalized by fluid conductivity, is

$$\frac{k_e}{k_f} = \epsilon + (1 - \epsilon)\kappa \quad (2.1)$$

where  $k_f$  is the fluid conductivity,  $\kappa = k_s/k_f$  is the ratio of solid to fluid conductivity, and  $\epsilon$  is the void fraction in the porous media. Similarly, the minimum effective conductivity is found in a serial layering of the solid and fluid phases,

$$\frac{k_e}{k_f} = \frac{1}{\epsilon + (1 - \epsilon)/\kappa} \quad (2.2)$$

Equations (2.1) and (2.2) act as theoretical upper and lower limits to true effective thermal conductivities of real material.

One of the most widely-used correlations was put forth by Zehner and Schlunder in 1970.<sup>176, 177</sup> They considered a cylindrically-shaped unit cell and made the analogy between

heat and mass transfer to derive an empirical fit to data in the bulk of two-phase porous media. The Zehner-Schlunder (ZS) correlation is

$$\frac{k_e}{k_f} = (1 - \sqrt{1 - \epsilon}) + \frac{2\sqrt{1 - \epsilon}}{1 - B/\kappa} \left[ \frac{(1 - 1/\kappa)B}{(1 - B/\kappa)^2} \ln\left(\frac{\kappa}{B}\right) - \frac{B + 1}{2} - \frac{B - 1}{1 - B/\kappa} \right] \quad (2.3)$$

where  $B$  is a deformation parameter related to porosity as

$$B = 1.25 \left( \frac{1 - \epsilon}{\epsilon} \right)^{1.11} \quad (2.4)$$

Following the success of the Zehner-Schlunder correlation, other researchers considered the specialized cases of high thermal conductivity ratio  $\kappa \geq 10^3$  when loads on the grains in the bed (due to either an external pressure or the grains own weight) resulted in large contact areas. In these cases, Zehner-Schlunder correlations under-predicted the actual effective conductivity.<sup>3</sup> An extensive review of correlations for effective thermal conductivity with consideration of contact between grains is provided by van Antwerpen *et al.*<sup>153</sup> Hsu *et al.* considered three lumped parameters models of varying two-dimensional unit cells for which they derived an effective conductivity. The first was for contact square-cylinders. The effective conductivity for this model is

$$\frac{k_e}{k_f} = \gamma_a \gamma_c \kappa + \frac{\gamma_a (1 - \gamma_c)}{1 + (1/\kappa - 1)\gamma_a} + \frac{(1 - \gamma_a)}{1 + (1/\kappa - 1)\gamma_a \gamma_c} \quad (2.5)$$

where Hsu *et al.* used the same fitting parameter of Nozad *et al.*,  $\gamma_c$ ,<sup>7</sup> they found best agreement with experimental data when  $\gamma_c = 0.01$ . The other geometric parameter is related to  $\gamma_c$  and  $\epsilon$  as

$$0 = \gamma_a^2 + 2\gamma_a \gamma_c (1 - \gamma_a) + \epsilon - 1 \quad (2.6)$$

Hsu *et al.*'s second correlation had the square-cylinder unit cell replaced with circular-cylinders. The correlation is given with dependence on conductivity ratios. For  $(1/\kappa - 1)\gamma_a < 1$ ,

$$\begin{aligned} \frac{k_e}{k_f} = & \gamma_c \gamma_a \kappa + \frac{1 - \gamma_a \sqrt{1 - \gamma_c^2}}{\gamma_a \gamma_c (1/\kappa - 1) + 1} + \frac{\kappa (\pi/2 - 2\theta_c)}{1 - \kappa} - \frac{2\kappa}{(1 - \kappa) \sqrt{1 - (1/\kappa - 1)^2 \gamma_a^2}} \\ & \times \left[ \tan^{-1} \left( \frac{\tan(\pi/4 - \theta_c/2) + (1/\kappa - 1)\gamma_a}{\sqrt{1 - (1/\kappa - 1)^2 \gamma_a^2}} \right) - \tan^{-1} \left( \frac{\tan(\theta_c/2) + (1/\kappa - 1)\gamma_a}{\sqrt{1 - (1/\kappa - 1)^2 \gamma_a^2}} \right) \right] \end{aligned} \quad (2.7)$$

For  $(1/\kappa - 1)\gamma_a > 1$ ,

$$\begin{aligned} \frac{k_e}{k_f} = & \gamma_c \gamma_a \kappa + \frac{1 - \gamma_a \sqrt{1 - \gamma_c^2}}{\gamma_a \gamma_c (1/\kappa - 1) + 1} + \frac{\kappa(\pi/2 - 2\theta_c)}{1 - \kappa} - \frac{\kappa}{(1 - \kappa) \sqrt{(1/\kappa - 1)^2 \gamma_a^2 - 1}} \\ & \times \left[ \ln \left( \frac{\tan(\pi/4 - \theta_c/2) + (1/\kappa - 1)\gamma_a - \sqrt{(1/\kappa - 1)^2 \gamma_a^2 - 1}}{\tan(\pi/4 - \theta_c/2) + (1/\kappa - 1)\gamma_a + \sqrt{(1/\kappa - 1)^2 \gamma_a^2 - 1}} \right) \right. \\ & \left. - \ln \left( \frac{\tan(\theta_c/2) + (1/\kappa - 1)\gamma_a - \sqrt{(1/\kappa - 1)^2 \gamma_a^2 - 1}}{\tan(\theta_c/2) + (1/\kappa - 1)\gamma_a + \sqrt{(1/\kappa - 1)^2 \gamma_a^2 - 1}} \right) \right] \end{aligned} \quad (2.8)$$

and for  $(1/\kappa - 1)\gamma_a = 1$

$$\frac{k_e}{k_f} = \frac{\gamma_c \gamma_a^2}{\gamma_a + 1} + \frac{1 - \gamma_a \sqrt{1 - \gamma_c^2}}{\gamma_c + 1} + \gamma_a (\pi/2 - 2\theta_c) - \tan(\pi/4 - \theta_c/2) + \tan(\theta_c/2) \quad (2.9)$$

where  $\gamma_c = 0.01$  was again found to fit best to experimental data. And the other geometric parameter relationship became

$$0 = 1 - \gamma_a \gamma_c - \frac{\gamma_a^2}{2} \left( \frac{\pi}{2} - 2\theta_c \right) \quad (2.10)$$

where the contact angle is  $\theta_c = \sin^{-1}(\gamma_c)$ . The last correlation of Hsu *et al.* came from three-dimensional unit cell extension of the square-cylinder to cubes,

$$\frac{k_e}{k_f} = 1 - \gamma_a^2 - 2\gamma_a \gamma_c + 2\gamma_a^2 \gamma_c + \gamma_a^2 \gamma_c^2 \kappa + \frac{\gamma_a^2 - \gamma_a^2 \gamma_c^2}{1 - \gamma_a + \gamma_a/\kappa} + \frac{2(\gamma_a \gamma_c - \gamma_a^2 \gamma_c)}{1 - \gamma_a \gamma_c + \gamma_a \gamma_c/\kappa} \quad (2.11)$$

where  $\gamma_c = 0.13$  fit best for cubes and the relationship between  $\gamma_c$ ,  $\epsilon$  and  $\gamma_a$  became

$$0 = (1 - 3\gamma_c^2)\gamma_a^3 + 3\gamma_c^2 \gamma_a^2 + \epsilon - 1 \quad (2.12)$$

Hsu *et al.* also proposed a correction to the ZS model for conductivity ratios of  $\kappa \geq 10^3$ . The assumption built into Zehner-Schlunder's model was of a point contact between grains in the bed. Incorporating the effects of finite-sized contact area, Hsu *et al.* corrected the ZS model as

$$\begin{aligned} \frac{\kappa_e}{\kappa_f} = & (1 - \sqrt{1 - \epsilon}) + \kappa \sqrt{1 - \epsilon} \left( 1 - \frac{1}{(1 + \alpha_0 B)^2} \right) \\ & + \frac{2\sqrt{1 - \epsilon}}{1 - B/\kappa + (1 - 1/\kappa)\alpha_0 B} \left[ \frac{(1 - 1/\kappa)(1 + \alpha_0)B}{(1 - B/\kappa + (1 - 1/\kappa)\alpha_0 B)^2} \ln \left[ \frac{1 + \alpha_0 B}{(1 + \alpha_0)B/\kappa} \right] \right. \\ & \left. - \frac{B + 1 + 2\alpha_0 B}{2(1 + \alpha_0 B)^2} - \frac{B - 1}{(1 - B/\kappa + (1 - 1/\kappa)\alpha_0 B)(1 + \alpha_0 B)} \right] \end{aligned} \quad (2.13)$$

where  $B$  is no longer found from as a simple deformation parameter but is instead related to  $\epsilon$  and  $\alpha_0$ . Hsu *et al.* found best agreement with experimental data when  $\alpha_0 = 0.002$  and  $\epsilon = 0.42$ .  $B$  can then be found from the solution of

$$0 = 1 - \frac{B^2}{(1-B)^6(1+\alpha_0B)^2} \left[ (B^2 - 4B + 3) + 2(1+\alpha_0)(1+\alpha_0B) \ln \left( \frac{(1+\alpha_0)B}{1+\alpha_0B} \right) + \alpha_0(B-1)(B^2 - 2B - 1) \right]^2 - \epsilon \quad (2.14)$$

Bauer and Schlunder<sup>14</sup> also improved on the earlier model of Zehner and Schlunder to include the additional effects of thermal radiation, gas heat transfer in the Knudsen regime, and finite-sized contact areas. The combined model, often called the Zehner-Bauer-Schlunder (ZBS) model is calculated as

$$\frac{k_e}{k_f} = (1 - \sqrt{1-\epsilon}) \epsilon \left[ (\epsilon - 1 + 1/\kappa_G)^{-1} + \kappa_r \right] + \sqrt{1-\epsilon} (\phi\kappa + (1-\phi)k_c) \quad (2.15)$$

where

$$k_c = \frac{2}{N} \left[ \frac{B(\kappa + \kappa_r - 1)}{N^2 \kappa_G \kappa} \ln \left( \frac{\kappa + \kappa_r}{B(\kappa_G + (1 - \kappa_G)(\kappa + \kappa_r))} \right) + \frac{B+1}{2B} \left( \frac{\kappa_r}{\kappa_G} - B \left( 1 + \frac{1 - \kappa_G}{\kappa_G} \kappa_r \right) \right) - \frac{B-1}{N \kappa_G} \right] \quad (2.16)$$

and

$$N = \frac{1}{\kappa_G} \left( 1 + \frac{\kappa_r - B\kappa_G}{\kappa} \right) - B(1 - 1/\kappa_G)(1 + \kappa_r/\kappa) \quad (2.17)$$

and  $B$  is given in Equation (2.4). Radiation is incorporated in  $\kappa_r$  parameter, given as

$$\kappa_r = \frac{4\sigma}{2/\epsilon_r - 1} \bar{T}^3 \frac{d_p}{k_f} \quad (2.18)$$

where  $\sigma$  is the Stefan-Boltzmann number ( $\sigma = 5.67 \times 10^{-8} \text{ W m}^{-2} \text{ K}^{-4}$ ),  $\epsilon_r$  is the emissivity of the material in the packing,  $d_p$  is the packing diameter (assumed spherical), and  $\bar{T}$  is the average, absolute temperature of the system (in K).

Effects due to interstitial gas in the Knudsen regime are defined by the term,  $\kappa_G$  given as

$$\kappa_G = \left[ 1 + \left( \frac{l}{d_p} \right) \right]^{-1} \quad (2.19)$$

where  $l$  is a modified mean free path of gas molecules,

$$l = 2 \frac{2 - \alpha_T}{\alpha_T} \left( \frac{2\pi \tilde{R}\bar{T}}{M_g} \right)^{1/2} \cdot \frac{k_f}{P(2c_p - \tilde{R}/M_g)} \quad (2.20)$$

where  $P$  is the gas pressure (in Pa),  $\tilde{R}$  is the universal gas constant (in  $\text{J mol}^{-1} \text{K}^{-1}$ ), and  $M_g$  is the molecular mass of the gas (in  $\text{kg mol}^{-1}$ ). The accommodation factor,  $\alpha_T$  is given by Bahrami *et al.* (originally given by Song & Yovanovich) as<sup>12,144</sup>

$$\alpha_T = \exp[-0.57T_r] \left( \frac{M^*}{6.8 + M^*} \right) + \frac{2.4\mu}{(1 + \mu)^2} [1 - \exp(-0.57T_r)] \quad (2.21)$$

where  $T_r = \frac{T_s - 273\text{K}}{273\text{K}}$ ,  $M^* = M_g$  for monatomic gases or  $M^* = 1.4M_g$  for diatomic gases, and  $\mu = \frac{M_g}{M_s}$  is the ratio of gas and solid molecular masses. The  $\alpha_T$  term, as described by Bahrami *et al.* represents the fraction of kinetic energy that a gas molecule leaves behind as thermal energy on a solid after collision.

In Figure 2.1, we see comparisons of effective conductivity predictions by the three models of Hsu *et al.*, Hsu *et al.* modification of ZS model, ZSB correction model, and their differences with the simple ZS correlation.

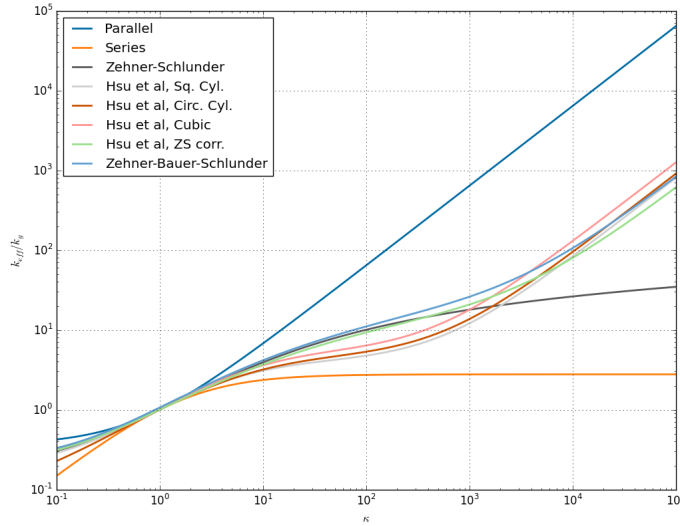


Figure 2.1: Models incorporating contact area demonstrate significant deviation from the Zehner-Schlunder correlation above  $\kappa > 10^3$ . All correlations are still bound by parallel and series approximations of the material.

Van Antwerpen compiled data from numerous publications to compare the accuracy of effective conductivity correlations.<sup>153</sup> For our discussion, I have also plotted the experimental data with all the correlations discussed above, given in Figure 2.2.

Near  $\kappa = 1$ , all correlations collapse to predict a  $\frac{k_e}{k_f} = 1$ , and experiments naturally match predictions. From the range of  $\kappa > 1$  to  $\kappa < 1000$ , experimental data is well-bound by the predictions of the simple ZS model and the complex two-dimensional models of Hsu *et al.*. Above  $\kappa > 1000$ , the ZS model, not taking into account heat transfer through finite-sized contacts, is no longer reliable as a model for  $k_{\text{eff}}$ . In high ranges of  $\kappa$ , the models incorporating contact-conduction in the granular material remain well-matched to experimental data. The results here show the worth of these general models for predictions of effective conductivity in some granular material.

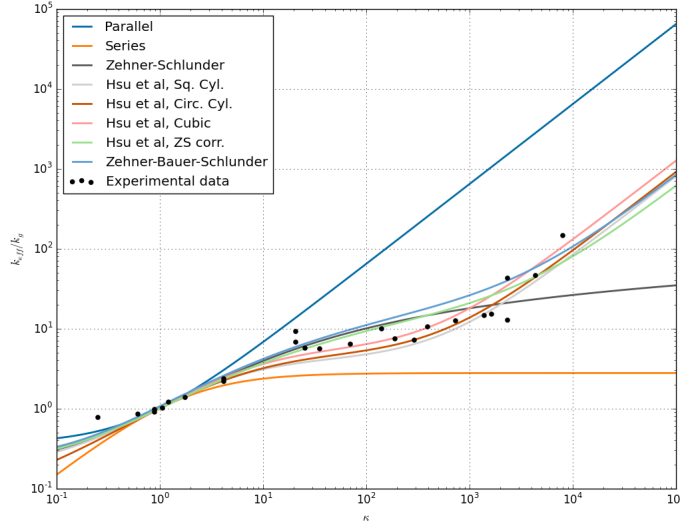


Figure 2.2: Comparison of  $k_{\text{eff}}$  correlations with compiled experimental data over a broad range of conductivity ratios,  $\kappa$ . Data compiled by<sup>153</sup> from many sources.

As part of the Ceramic Optimal Material Experiments for Thermomechanics (COMET) project at UCLA, we measured the effective conductivity of  $d_p = 1$  mm graphite (IG11) pebbles for 135 °C to 544 °C. The results will be discussed in more detail later, though the results will be presented here for comparison with the correlations; Figure 2.3 shows the COMET data. The measured conductivity from COMET is well above the lower bounds of series approximation for effective conductivity, though is just below the lowest values predicted

from Hsu *et al.*'s square-cylinder two-dimensional model. We attribute the smaller values of effective conductivity on the surface roughness of the graphite pebbles in conjunction with their small size and small mass. In short, however, the measurements of COMET are also demonstrative of the inaccuracies in general predictions of granular material thermal properties.

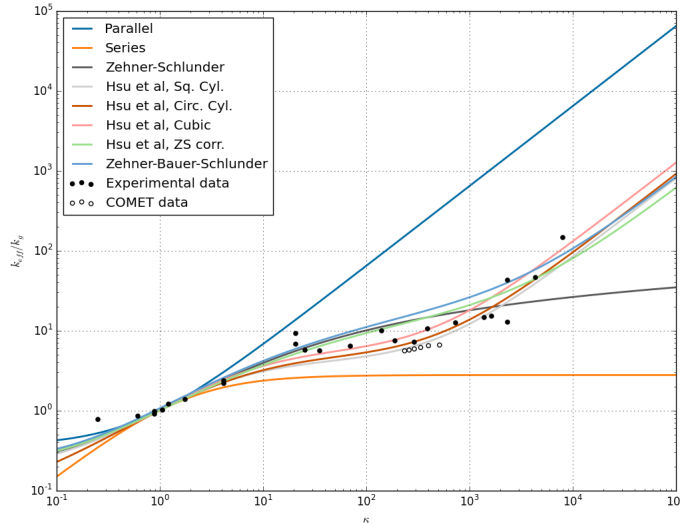


Figure 2.3: Comparison of COMET data on IG11 graphite,  $k_{\text{eff}}$  correlations, and experimental data. Data compiled by<sup>153</sup> from many sources and measured data at UCLA.

## 2.2.2 Convection in Granular Media

Before discussing the correlations for Nusselt number of particles with forced convection in two-phase porous media, I will consider a simple case of an axisymmetric sphere completely immersed in a quiescent fluid. The steady-state energy equation of the fluid surrounding the sphere is

$$\frac{\partial}{\partial r}(k_f r^2 T) = 0 \quad (2.22)$$

for which the solution is

$$T = -\frac{C_1}{r} + C_2 \quad (2.23)$$

subjected to a boundary condition of

$$k_f \frac{\partial T}{\partial r} \Big|_R = -h(T_R - T_f) \quad (2.24)$$

where  $T_R$  is the temperature of the fluid in contact of the sphere of radius  $R$  and  $T_f$  is the temperature of the fluid infinitely far away from the sphere – which naturally leads to the second boundary condition of  $T(r \rightarrow \infty) = T_f$ . These two boundary conditions yield a temperature solution of

$$T = \frac{hR}{k_f} \frac{R}{r} (T_R - T_f) + T_f \quad (2.25)$$

We can also say  $T(r = R) = T_R$  to show,

$$T_R = \frac{hR}{k_f} \frac{R}{R} (T_R - T_f) + T_f \quad (2.26)$$

or simply

$$\frac{hR}{k_f} = 1 \quad (2.27)$$

The Nusselt number for a sphere is defined as

$$\text{Nu}_p = \frac{hd_p}{k_f} \quad (2.28)$$

which is simply

$$\text{Nu}_p = 2 \frac{hR}{k_f} = 2 \quad (2.29)$$

showing that in the limit of  $\text{Re}_p \rightarrow 0$ , the Nusselt number for a sphere in fluid will asymptotically approach  $\text{Nu}_p = 2$ . This value is a natural limit for a Nusselt number correlation for particle-to-fluid heat transfer.

### 2.2.2.1 Nusselt number correlations for an individual sphere

For a particle falling through a fluid or a fluid moving past a single particle, a number of correlations exist for the Nusselt number of that individual sphere. One common correlation is from Ranz & Marshall,<sup>124</sup> developed from heat and mass transfer analogies with experiments on evaporating drops. Their correlation is

$$\text{Nu}_p = 2.0 + 0.6\text{Pr}^{1/3}\text{Re}_p^{1/2} \quad (2.30)$$

Generally considered valid for  $\text{Re}_p < 200$ . The Ranz & Marshall correlation is used by Sasdisi et al. in a CFD-DEM study of heat transfer in 2D fluidized spouts.<sup>147</sup> Romkes et al. did direct CFD studies of particle-to-fluid heat transfer and validated against Ranz & Marshall;<sup>135</sup> though they noted the correlation was valid over particle Reynolds numbers of  $10 < \text{Re}_p < 10^4$ . Wu et al. also employed the correlation in a DEM study of granular material.<sup>168</sup> Li & Mason studied the correlation against their CFD-DEM studies,<sup>101</sup> they found the RM correlation to be adequate for small  $\text{Re}_p < 200$  also.

Gnielinski<sup>72</sup> developed a semi-empirical method where the Nusselt number for an arbitrary shape is related to the solution for a flat plate with appropriate transformations of the length scale. The solution is a function of the asymptotic laminar, turbulent, and  $\text{Re}_p \rightarrow 0$  solutions,

$$\text{Nu}_p = 2 + \sqrt{\text{Nu}_{lam}^2 + \text{Nu}_{tur}^2} \quad (2.31)$$

where

$$\text{Nu}_{lam} = 0.664\text{Re}_p^{1/2}\text{Pr}^{1/3} \quad (2.32)$$

and

$$\text{Nu}_{turb} = \frac{0.037\text{Re}_p^{0.8}\text{Pr}}{1 + 2.443\text{Re}_p^{-0.1}(\text{Pr}^{2/3} - 1)} \quad (2.33)$$

The two single-particle correlations are shown over a range of Reynolds numbers in Figure 2.4. The two correlations are in good agreement near low Reynolds number.

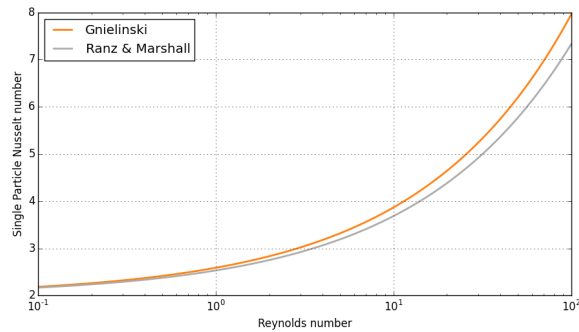


Figure 2.4: Comparison of correlations for Nusselt number of a single spherical particle in forced flow.

### 2.2.2.2 Nusselt number correlations for a sphere as part of a packing

However, this correlation was developed from measurements of a single particle in flow. The influence of neighboring grains will disrupt the flow field and result in a different Nusselt number. Thus, for the Nusselt number for a single grain in a packed bed,  $\text{Nu}_i$ , is often related to the Nusselt number of a single particle (alone in an infinite fluid),  $\text{Nu}_p$ , via the packing fraction. The subscripts  $i$  and  $p$  will be used consistently below to signify the Nusselt for a particle in a packing or a correlation for a single particle.

The data of Ranz suggested the following for spherical particles in a fixed bed

$$\text{Nu}_i = 2 + 1.8\text{Re}_p^{0.6}\text{Pr}^{1/3} \quad (2.34)$$

Another commonly-cited correlation is that of Wakao *et al.*<sup>165,166</sup> Combining a large amount of data over a broad range of particle Reynolds numbers and Prandlt numbers found a fitting function of

$$\text{Nu}_i = 2 + 1.1\text{Re}_p^{0.6}\text{Pr}^{1/3} \quad (2.35)$$

Flueckiger *et al.*<sup>54–56</sup> as well as Yang & Garimella,<sup>172</sup> both implemented the Wakao *et al.* correlation in their studies of heat transfer in solar thermal storage tanks.

Zhou *et al.*<sup>187</sup> used a modified form from Kunii and Levenspiel, to fit their experimental data. They gave

$$\text{Nu}_i = 2 + 1.2\text{Re}_p^{1/2}\text{Pr}^{1/3} \quad (2.36)$$

In another study, Li & Mason<sup>102</sup> also employed a modified form of Ranz & Marshall to account for the packing in the assembly with a function of void fraction in front of the Reynolds and Prandtl terms,

$$\text{Nu}_i = 2 + 0.6\epsilon^n\text{Re}_p^{1/2}\text{Pr}^{1/3} \quad (2.37)$$

where they found  $n = 3.5$  fitting for 3 mm pellets in dilute flows.<sup>102</sup> Kloss *et al.*<sup>95</sup> and Di Maoi *et al.*<sup>42</sup> also use the modified Ranz & Marshall correlation provided by Li & Mason in their CFD-DEM studies. This correlation, however, conflicts with the correlations of Ranz, Wakao, and the Kunii & Levenspiel. In the asymptotic limit of  $\epsilon \rightarrow 1$ , the correlation

correctly approaches the single particle correlation of Ranz & Marshall, Equation (2.30). For a dense packing,  $\epsilon = 0.36$ , the correlation gives

$$\text{Nu}_i = 2 + 0.0168\text{Re}_p^{1/2}\text{Pr}^{1/3} \quad (2.38)$$

which is significantly less than any of the correlations of Equations (2.34) to (2.36)

Achenbach defined an empirical arrangement factor,  $f(\epsilon) = 1 + 1.5(1 - \epsilon)$  to relate the single particle Nu of Gnielinski, Equation (2.31), to a sphere in a packing,

$$\text{Nu}_i = (1 + 1.5(1 - \epsilon)) \text{Nu}_p \quad (2.39)$$

The modified form of Achenbach was used in a CFD-DEM study by Rickelt *et al.*,<sup>133</sup> which covers  $\text{Re}_p$  up to  $10 \times 10^5$  and  $\text{Pr}$  from 0.7 to  $7 \times 10^4$ . The Gnielinski correlation<sup>72</sup> is also used in the ANSYS calculations of helium-cooled pebble bed breeders, reported by Hernandez *et al.*,<sup>81</sup> Cismondi *et al.*,<sup>33</sup> Poitevin *et al.*,<sup>122</sup> etc. However, Visser notes<sup>164</sup> that the correlation of Gnielinski is valid for  $\text{Re}_p$  in 500 to 1000, for  $\epsilon$  in the range 0.26 to 1.0. Thus he uses the correlation of Gunn for his situation of lower Reynolds number<sup>76</sup>

$$\text{Nu}_i = (7 - 10\epsilon + 5\epsilon^2)(1 + 0.7\text{Re}_p^{0.2}\text{Pr}^{1/3}) + (1.33 - 2.4\epsilon + 1.2\epsilon^2)\text{Re}_p^{0.7}\text{Pr}^{1/3} \quad (2.40)$$

which Gunn developed to be valid for: heat transfer to particles at low and high Reynolds number, at low and high porosities; single particle at low Reynolds number, particles and particles in ensembles with high Reynolds number and moderate Prandtl. Amritkar *et al.* also employ the Gunn correlation in their simulations of spout-fluidized flow.<sup>4</sup>

The correlations are given as functions of Re at a specified value of  $\epsilon = 0.36$  and  $\text{Pr} = 0.7$  in Figure 2.5. We see the correlation from Li & Mason (a modified form of Ranz & Marshall), from Equation (2.37), predicts very small Nusselt numbers over this entire range of Reynolds number. Additionally, the modified Gnielinski of Equation (2.39) and the correlation of Gunn in Equation (2.40) predict much higher Nusselt numbers at low Reynolds number than any other correlation, and are well above the single particle limit of  $\text{Nu} = 2$  when  $\text{Re} \rightarrow 0$ . In the studies of Achenbach and Rickelt, which employed the modified Gnielinski studies, the authors were interested in larger Reynolds number regimes. Above  $\text{Re} > 10$ , Gnielinski

correlation is similar to Wakao and Ranz correlations, thus the over-prediction at very small  $Re$  may not have been observed. Gunn rejects the notion that the Nusselt number should approach 2 in the no-flow limit.<sup>76</sup> The discrepancy appears to arise because of definitions of either particle or bed heat transfer coefficients. It seems Gunn's definition was meant for representative cross sections of packed beds with voidage defined by the void fraction rather than for an individual particle communicating with forced flow in a packed bed.

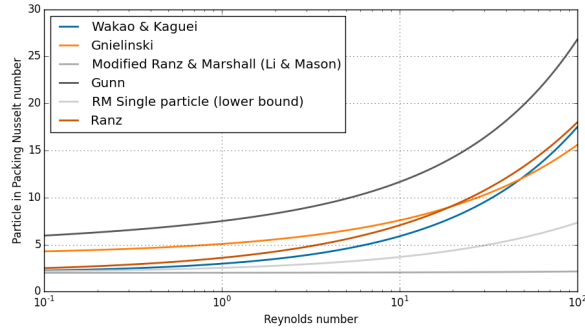


Figure 2.5: Comparison of correlations for Nusselt number of a single spherical particle in forced flow.

After discussing many popular correlations for Nusselt number in packed beds, considering the very small Reynolds number ( $Re \sim 1$ ) and packing fraction expected with the purge gas of helium in tritium breeders, the correlation of Wakao *et al.*, as given in Equation (2.35), is sufficient. However, we note the debate that still exists in literature for determining Nusselt number for a specific particle in a packed bed. If experimental validation shows the Wakao correlation to be inaccurate, we will revisit the implementation in our modeling.

### 2.2.3 Radiation in Granular Media

The temperatures expected in the solid breeder are high enough radiation between grains may be important. The radiation exchange between contacting neighbors in a packed bed becomes extremely complex due to the local and semi-local nature of radiation. A standard approach to treat radiation exchange between surfaces is to consider the view factor between them. In a dense, randomly packed bed of spheres the computation of view factors between

pebbles can be done via a method such as that proposed Feng and Han.<sup>52</sup>

The ZSB model incorporates radiation heat transfer into the general expression and calculation of  $k_c$  and  $N$ . Others have attempted to incorporate radiation into an effective thermal conductivity and typically it is done with a superposition of gas/solid conduction models (such as all those described above) with a separate radiation model. One common technique is to analyze a representative unit cell with a thermal radiative conductivity of a general form,

$$k_e^r = 4F_E^*\sigma d_p \bar{T}^3 \quad (2.41)$$

where  $F_E^*$  is a radiation exchange factor. Van Antwerpen *et al.* describe many researchers' techniques for defining the radiation exchange factors and the simplifications that must appear to allow a closed solution to complicated equations. I will focus on one commonly-used correlation from Breitbach & Barthels.<sup>20</sup>

Breitbach & Barthels began with the unit cell defined by Zehner & Schlunder, though noted that the closed cell precluded radiation from voids outside the cell volume. Therefore they modified the correlation via closing the bases of the unit cells with black surfaces instead of with surfaces of the same emissivity as the grains in the bed. The result is given as the BB correlation,<sup>20</sup>

$$F_E^* = \left[ (1 - \sqrt{1 - \epsilon}) \epsilon + \frac{\sqrt{1 - \epsilon}}{2/\epsilon_r - 1} \cdot \frac{B + 1}{B} \cdot \frac{1}{1 + \frac{1}{(2/\epsilon_r - 1)\Lambda_f}} \right] \quad (2.42)$$

where  $B$  is again given by Equation (2.4), and  $\Lambda_f = \frac{k_s}{4d_p\sigma\bar{T}^3}$  is a dimensionless solid conductivity for the granular packing.

An IAEA technical report provides effective conductivity measurements of  $d_p = 60$  cm graphite pebble beds.<sup>132</sup> The data is used to compare against the combined correlations of ZS and BB. The  $k_{\text{eff}}$  measurements in Helium are given in Figure 2.6, measurements in Nitrogen are given in Figure 2.7. We see that the effective thermal conductivity correlations are significantly under-predicting, over the entire range of temperatures, when compared to experimental values. For the graphite pebble beds measured in the SANA report, we consider the Grashof number for the packing. The Grashof number is indicative of natural

convection effects in the voids. The Grashof number is written as

$$\text{Gr} = \frac{g\beta(T_s - T_0)l^3}{\nu_f^2} \quad (2.43)$$

where we estimate it in voids of size  $l = \frac{d_p}{2}$ , a temperature drop of  $T_s - T_0 = 10\text{ K}$  is an lower estimate. The kinematic viscosity,  $\nu_f$  of the gases is known, and thermal expansion of an ideal gas is  $\beta = \frac{1}{T}$ . Let us assume a situation where temperatures and materials are all identical and the only variation is in length. Grashof numbers for these cases would be

$$\frac{\text{Gr}_1}{\text{Gr}_2} = \left(\frac{l_1}{l_2}\right)^3 \quad (2.44)$$

Zehner & Schlunder derived their correlation from mass-diffusion experiments of Curie.<sup>35</sup> The data of Curie was done primarily on grains of around 1 mm. Thus comparing  $\frac{l_1}{l_2}$  between the size of particles for which the ZS correlation was derived and particles for which it was applied for SANA data yields

$$\frac{\text{Gr}_1}{\text{Gr}_2} \sim 10^{-6} \quad (2.45)$$

With a Grashof number significantly higher for the SANA experiments, it is indicative that the amount of natural convection present in the SANA experiment will have a much greater impact on heat transfer than the ZS correlation, derived on data for stagnant inter-stitial gas, is able to predict. This demonstrates limited applicability of effective conductivity correlations for packed bed conditions different from those for which the correlations were derived.

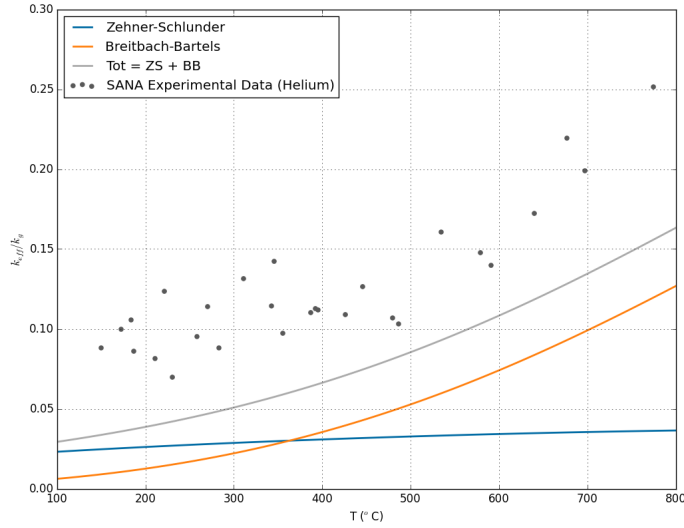


Figure 2.6: Comparison of SANA data in Helium gas with Zehner-Schlunder and Breitbach-Bartels correlations. Data from IAEA Tecdoc-1163.<sup>132</sup>

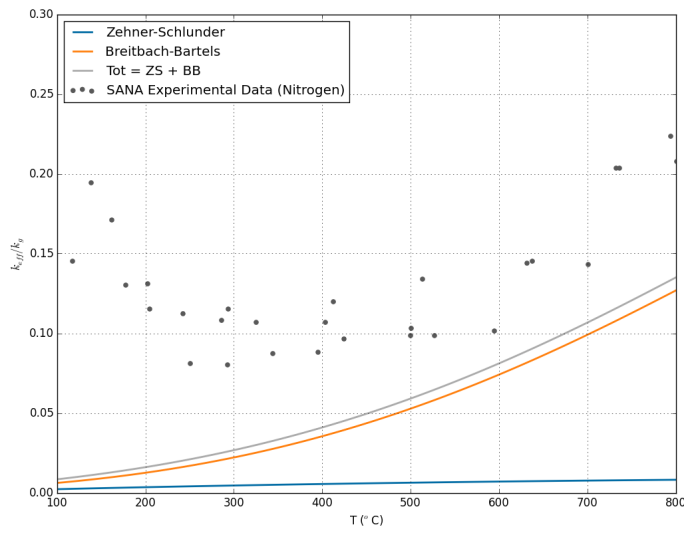


Figure 2.7: Comparison of SANA data in Nitrogen gas with Zehner-Schlunder and Breitbach-Bartels correlations. Data from IAEA Tecdoc-1163.<sup>132</sup>

## 2.3 Momentum Transfer in Packed Beds with Fluid Flow

Present three major correlations for pressure drop and drag force for fluid flow in packed beds and discuss their range of applicability.

P.C. Carman,<sup>24</sup> using Kozeny's Equation as a starting point, derived a formula for the

average velocity of a laminar flow through a randomly packed beds at the close-packed limit,

$$\bar{U} = \left( \frac{L}{L_e} \right)^2 \frac{\epsilon^3}{k_0 \mu S^2} \frac{\Delta p}{L} \quad (2.46)$$

where  $\mu$  is the viscosity, Carman called the tortuosity ( $L_e/L$ ) the ratio of the actual path of a streamline through the pore space,  $L_e$ , to the length of packing,  $L$ .  $S$  is the particle surface area per unit volume of the bed. For a bed of spheres this is  $S = 6(1 - \epsilon)/d_p$ ,  $\epsilon$  is the void fraction, and constant,  $k$ , varies between materials and packings but for regular spheres is found experimentally to be  $k \approx 5.0$ . The pressure drop per unit length of flow is  $\Delta p/L$ .

We rearrange Equation (2.46) as

$$\frac{\Delta p}{L} = \frac{180 \bar{U} \mu}{d_p^2} \frac{(1 - \epsilon)^2}{\epsilon^3} \quad (2.47)$$

The pressure gradient acting upon the fluid in the packed bed must be balanced by the drag force of all the particles in the bed. If we assume some average force,  $\langle f \rangle$ , as the ensemble average of the particle drag forces, we can write

$$\frac{\Delta p}{L} = n \langle f \rangle \quad (2.48)$$

where  $n$  is the number density of particles in the bed. We relate the number density in terms of the packing fraction as

$$n = \frac{6\phi}{\pi d_p^3} = \frac{6(1 - \epsilon)}{\pi d_p^3} \quad (2.49)$$

Thus the average drag per particle in this flow is

$$\langle f \rangle = \frac{\Delta p}{L} \frac{\pi d_p^3}{6(1 - \epsilon)} \quad (2.50)$$

We will nondimensionalize the average drag force based on the classic Stokes force – the drag force of a single particle in unbounded fluid,

$$F = \frac{\langle f \rangle}{3\pi\mu d_p U} \quad (2.51)$$

and when we plug in Equation (2.50) to Equation (2.51) we have

$$F_{kc} = \frac{\Delta p}{L} \frac{\pi d_p^3}{6(1 - \epsilon)} \frac{1}{3\pi\mu d_p U} \quad (2.52)$$

which, with the substitution of the Kozeny-Carman pressure (Equation (2.47)), becomes

$$F_{kc} = \frac{180U\mu}{d_p^2} \frac{(1-\epsilon)^2}{\epsilon^3} \frac{\pi d_p^3}{6(1-\epsilon)} \frac{1}{3\pi\mu d_p U} \quad (2.53)$$

or simply

$$F_{kc} = 10 \frac{1-\epsilon}{\epsilon^3} \quad (2.54)$$

Carman himself<sup>25</sup> points out the limitations of applicability of the Kozeny-Carman (KC) equation: built into the equation is the assumption that the range of pore size and shape is fairly isotropic and similarly the tortuosity through the packed bed is relatively uniform. In the form we have used with Equation (2.54), we have also assumed spherical particles in random packing near the close-packed limit ( $\phi \rightarrow 0.64$ ) with laminar flow at low Reynolds numbers. Carman provided modifications to cases of extremely high porosity and non-spherical, non-regular packings in his book from 1956.<sup>25</sup>

Another correlation that is perhaps more commonly used in general is the Ergun equation.<sup>49</sup> Ergun's equation is an empirical fit to a vast amount of experimental data. His pressure drop per length is

$$\frac{\Delta p}{L} = \frac{150U\mu}{d_p^2} \frac{(1-\epsilon)^2}{\epsilon^3} + \frac{1.75\rho U^2}{d_p} \frac{1-\epsilon}{\epsilon^3} \quad (2.55)$$

We nondimensionalize the Ergun equation of Equation (2.55) by Stokes flow solution, as done to derive Equation (2.54), to find

$$F_e = 8.33 \frac{1-\epsilon}{\epsilon^3} + 0.18 \frac{\text{Re}}{\epsilon^3} \quad (2.56)$$

where we see the Reynolds number dependence in the second term on the right side of Equation (2.56). Comparing this to the nondimensionalized drag force of the Kozeny-Carman relation (Equation (2.54)), we see that the first term on the right hand side is essentially the same but Ergun's equation underpredicts Stokes flow by roughly 20% (comparing the leading coefficient of 8.33 to 10.0). This is understandable as Ergun's equation was meant to fit a wide range of flow (finite-to-large Re), including turbulent flow, whereas the Kozeny-Carman was meant specifically to apply to Stokes flow-type laminar packed beds.

Koch, Hill, & Ladd studied packed bed flow with high-precision lattice-Boltzmann simulations to develop correlations for drag in a packed bed over a wide range of packing fractions and Reynolds numbers.<sup>83,84,96</sup> They studied ordered arrays of spheres at various flow angles with dilute arrays (interstitial Reynolds number greater than particle Reynolds number), up to dense ordered arrays, and random arrays.

They consider the drag force as a sum of viscous and inertial stresses. Based on scaling arguments, the viscous and inertial contributions to  $F$  are expected to be independent of  $\text{Re}$  and linearly proportional to  $\text{Re}$ , respectively (in much the same form as Ergun's empirical fit of Equation (2.56)). Thus their numerical results were fit to the form

$$F = F_0(\phi) + F_3(\phi)\text{Re} \quad (2.57)$$

where, from their lattice-Boltzmann simulations they found,

$$F_0 = \begin{cases} \frac{1+3(\phi/2)^{1/2}+(135/64)\phi\ln\phi+16.14\phi}{1+0.681\phi-8.48\phi^2+8.16\phi^3} & \text{if } \phi < 0.4 \\ 10.0 \frac{\phi}{(1-\phi)^3} & \text{if } \phi > 0.4 \end{cases} \quad (2.58)$$

and

$$F_3 = 0.0673 + 0.212\phi + 0.0232 \frac{1}{(1-\phi)^5} \quad (2.59)$$

Koch, Hill, & Ladd<sup>18,74,83,96</sup> also compared their results with data from experiments. They found that at smaller Reynolds number and larger solid volume fractions, the rate of increase of drag force increases with the Reynolds number in much the same way predicted by Ergun's equation. However, at solid volume fractions smaller than those that can be achieved in physical experiments, at the largest Reynolds numbers, the rate of drag force increase is significantly smaller than the value predicted by Ergun's equation.

For Stokes-flow (and near-Stokes-flow), the drag force computed from their lattice-Boltzmann simulations were indistinguishable from experimental data over all ranges of packing fractions achievable in controlled experiments. Their correlation for small Reynolds number and large packing fraction is simply the Kozeny-Carman relationship – which was itself generated with coefficients matching experimental data so it is no surprise their correlation fits that phase space of  $\phi - \text{Re}$ .

Three correlations relating a nondimensional drag force to packing fraction and Reynolds number have been presented. The first, the Kozeny-Carman equation, Equation (2.54), was derived assuming small Reynolds numbers with a broad range of packing fraction. The second, the Ergun equation, Equation (2.56), is meant to be applicable over a broad range of Reynolds number due to its origins as an empirical fit from experimental data but, by the same token, is limited to experimentally attainable packing fractions. Finally, the third correlation by Koch, Hill, & Ladd (KHL), Equations (2.57) to (2.59) was numerically developed to provide drag correlations over a much more broad packing fraction and Reynolds numbers than is possible with physical experiments.

Here I provide a graphical comparison of the relationships that compares the three correlations: KC, Ergun, and KHL.

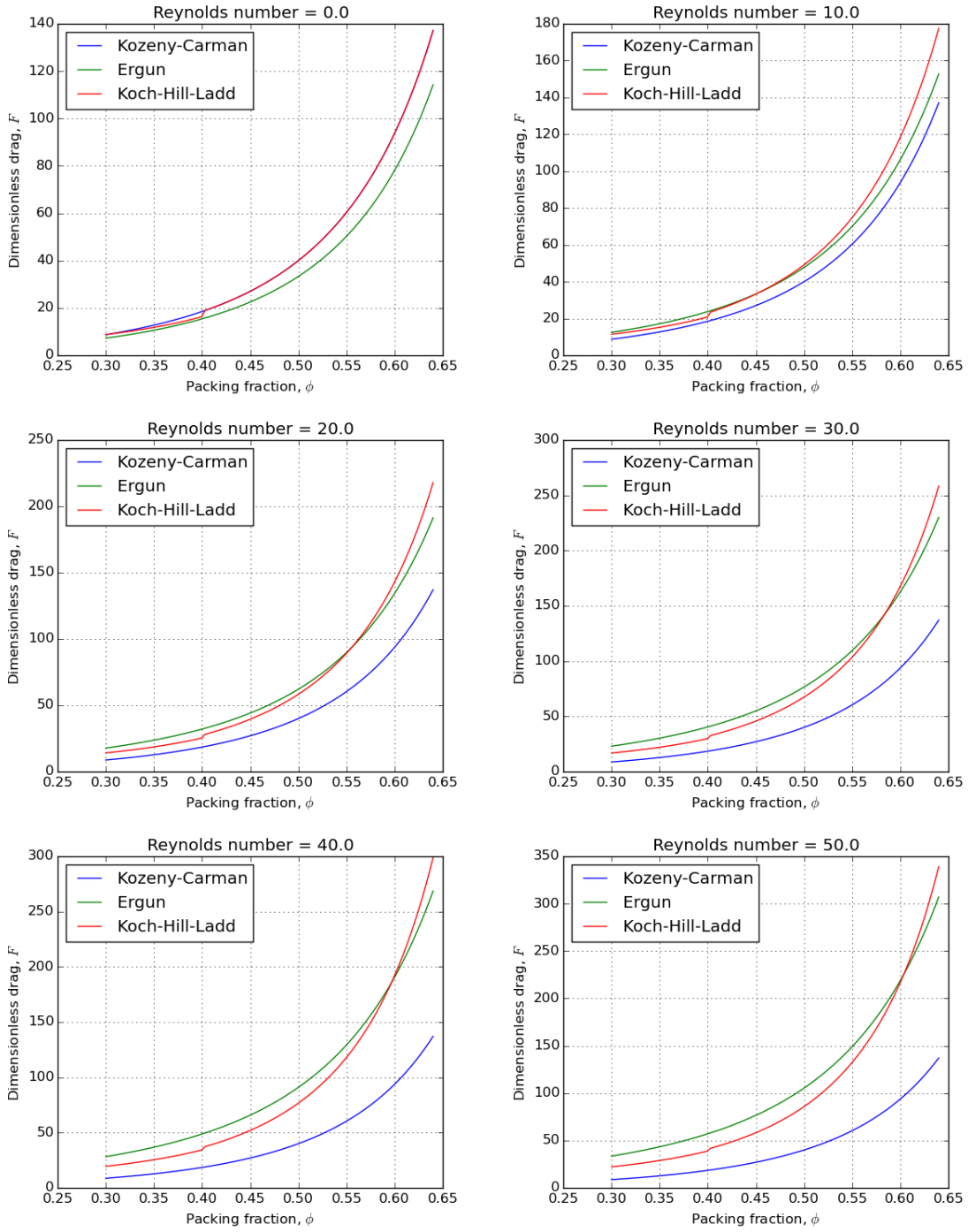


Figure 2.8: Comparison of pressure drop correlations over a range of packing fractions and Reynolds numbers.

## 2.4 Status of Ceramic Breeder Modeling and Analysis

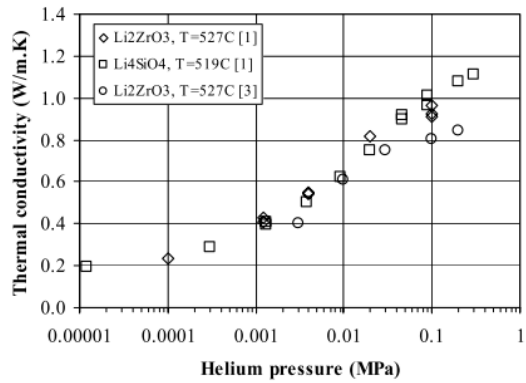
Research efforts have been aimed at developing an understanding and characterization of thermomechanics of ceramic breeder pebble beds. Such an understanding is essential to providing confidence in performance and lifetime of ceramic breeder blanket designs. In particular, a significant effort of pebble bed thermomechanical studies is development of modeling simulation tools. In this section I will discuss the current state of modeling – and experimental work feeding into modeling efforts – for ceramic breeders of tritium.

### 2.4.1 Experiments to Develop Constitutive Equations for Pebble Beds

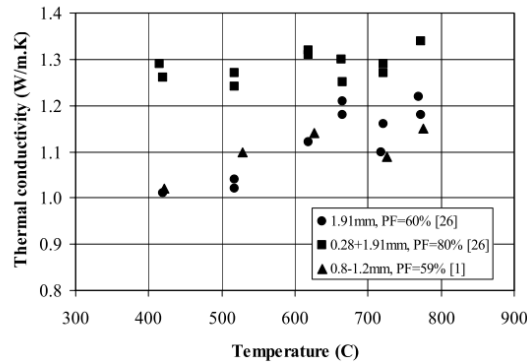
Many experiments have been run to measure the effective thermal conductivity of a volume of ceramic pebbles. In Figure 2.9, the effective conductivity is seen to be strongly affected by the interstitial gas but weakly affected by the mechanical loads on the bed. The main conclusions to bear in mind from Figure 2.9 are that: 1) the interstitial gas is an important transporter of heat in the bed and 2) the effective thermal conductivity of the pebble bed is low and will limit the size of the ceramic pebble bed volume to satisfy the temperature window mentioned above.

Reimann *et al.* have conducted an extensive experimental study of stress-strain relations of ceramic breeder pebble beds using an oedometric test apparatus.<sup>119, 127, 128, 130, 131</sup> The most significant macroscopic experimental phenomena witnessed in pebble beds is an irreversible plastic strain when load is removed, a non-linear elasticity, a pressure-dependent plasticity, and volumetric creep. A particularly noticeable feature, clearly demonstrated in Figure 2.10, is the reduced amount of irreversible strain when subjected to additional loading cycles after the first unloading. This may suggest the existence of a semi-equilibrium packing state in the pebble bed which can be reached after applying a pre-load to account for the large strain in the first cycle of a pebble bed. This semi-equilibrium packing state is a feature which may be advantageous for use in a fusion reactor.

To study temperature effects in Reimann's studies, beds are freely heated to desired working temperatures before pressure load is applied. Under the same loading condition,



(a) Effective conductivity of ceramic pebble beds is dependent on the pressure of the interstitial gas, a minimum of about  $k_{\text{eff}} = 0.2 \text{ W m}^{-1} \text{ K}^{-1}$  in vacuum.



(b) The effective conductivity of pebble beds is weakly dependent on external mechanical pressure and is always approximately  $k_{\text{eff}} = 1 \text{ W m}^{-1} \text{ K}$  in helium.

Figure 2.9: Effective conductivity of lithium ceramics. Results from Ref.<sup>2</sup>

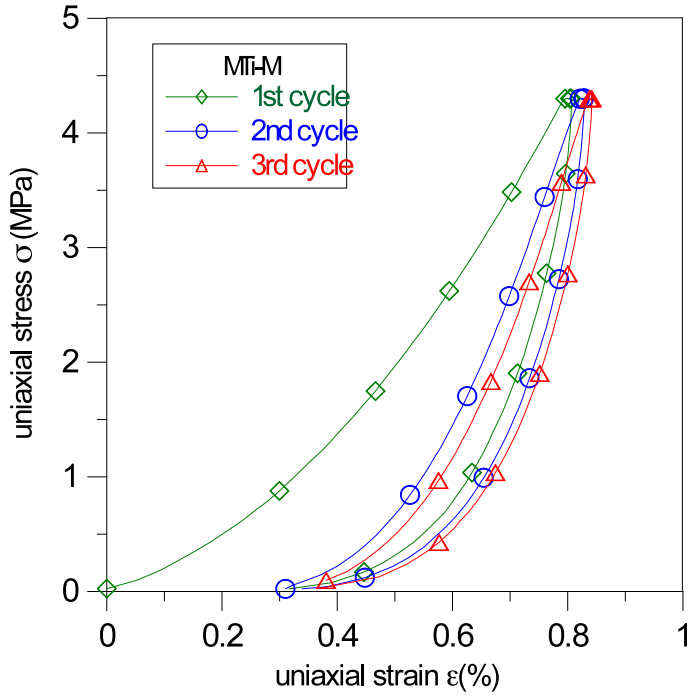


Figure 2.10: Example of uniaxial compression testing results for lithium metatitanate pebble bed.<sup>156</sup>

beds behave much softer at higher temperatures. The bed stiffens as the pressure increases. An illustration of this phenomenon is presented in Figure 2.11 for a lithium orthosilicate pebble bed between 50 °C to 850 °C. At higher temperatures (such as > 650 °C), a creep-like behavior becomes apparent. Creep behavior allows the pebble bed to relax and sustain higher stresses, however at elevated temperatures we must keep in mind issues of surface sintering of pebbles. The data was used to correlate creep rate as a function of temperature, stress, and time for both lithium orthosilicate, lithium metatitanate, and beryllium pebble beds.<sup>22, 129, 131</sup>

Coming from the standpoint that strain in a pebble bed is induced by thermal expansion, an experiment was conducted to characterize the pebble bed thermal expansion coefficient.<sup>148</sup> The thermal expansion coefficient of a packed  $\text{Li}_2\text{TiO}_3$  pebble bed is measured under a compressive load of 0.1 MPa. The study concludes that for beds with packing factors of 65.3 to 68.5%, the average thermal expansion coefficient was  $(1.4 \pm 0.2) \times 10^{-5} K^{-1}$ . This thermal expansion coefficient of the pebble bed was equal to 78% of that for the bulk material under

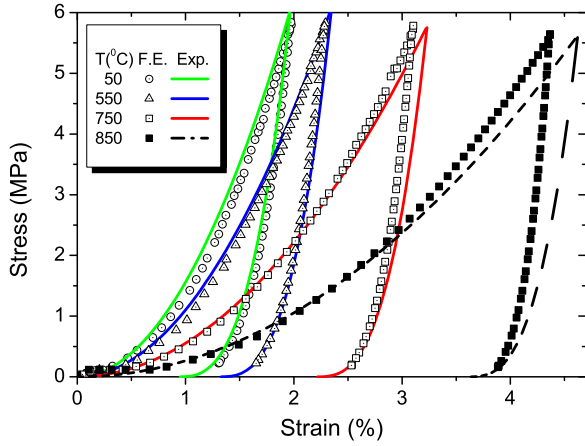


Figure 2.11: Example of uniaxial compression testing results compared with predictions from material constitutive equations for lithium orthosilicate pebble beds at different temperatures.<sup>63</sup>

the conditions used in the study. The reduction in thermal expansion coefficient is less significant than that of the effective modulus, which is more than 2 orders of magnitude smaller than the bulk value.

The effect of thermal cycling on the packing state is of interest; in particular, it is foreseen that the ITER TBM will be subjected to such conditions. The question that arises is whether a void region will be created under thermal-cyclic loading due to the differential rates of expansion and contraction of the pebble bed and structural containing wall. This uncertainty was first addressed in an experimental set-up involving  $\text{Li}_2\text{TiO}_3$  pebbles enclosed by two Kovar flanges while sandwiched between two commercial-grade CVD silicon carbide discs.<sup>23</sup> The set-up allows for generating a high stress through large differential in thermal expansion coefficients. The experimental results indicate that high thermal stresses and deformations are present during the initial thermal cycle of the assembled test article, but are successively alleviated due to a combination of pebble re-arrangement within the bed and creep induced deformation. This suggests that a few thermal cycles under a controlled atmosphere and a compressive load before final assembly of blanket sections would mitigate the severity of the thermal stresses during start-up. This is also shown in a later experiment, in which the

increment of compression decreased with each heating cycle and became negligible after 30 cycles.<sup>149</sup> Extrapolating the finding to a prototypical blanket breeder pebble bed design, the study concludes that for a height of 1 m long pebble bed, a 51 mm high cavity may be generated at the top of the bed with an initial packing of 65% under thermal cyclic operations.

Zhang *et al.* ran similar cyclic pressure experiments to illuminate the existence of more steady stress-strain responses of packed beds under different pressures.

#### 2.4.1.1 Post-irradiation experiments at Petten

The pebble bed assemblies (PBA) experiment is designed to study the effect of neutron irradiation on the thermomechanical behavior of a ceramic breeder pebble-bed under DEMO representative thermomechanical loads.<sup>107</sup> This was accomplished via analysis of changes of the in-pile temperature profiles during irradiation as well as from the post irradiation examination of the pebble bed in the Hot Cells. Within the assemblies, there are four test elements; each resembling a small-scale mock-up of a HCPB TBM with a ceramic breeder pebble bed sandwiched between two beryllium pebble beds. Before irradiation, the beds are pre-compacted with a compressive load of 3 MPa to ensure good settling and contact.

FEM analysis was performed to study pre-compaction procedures. During progressive irradiation, temperatures are recorded at several locations in the ceramic breeder bed as well as other critical positions. Reviewing the recorded temperature data, when comparing the temperature in the center of the ceramic breeder pebble bed during later cycles and earlier cycles there appears to be a decrease in temperature for the exact same environmental conditions. Changes in the pebble beds and their characteristics are examined both in-pile by neutron radiography and out-of-pile by e.g. SEM during post-irradiation examination (PIE). The estimated bed height reduction from neutron radiographies over the course of the irradiation has shown 3% of creep compaction.

A pebble bed experiencing creep compaction is both becoming more dense as well seeing more-developed inter-pebble conduction paths. The effective thermal conductivity for a

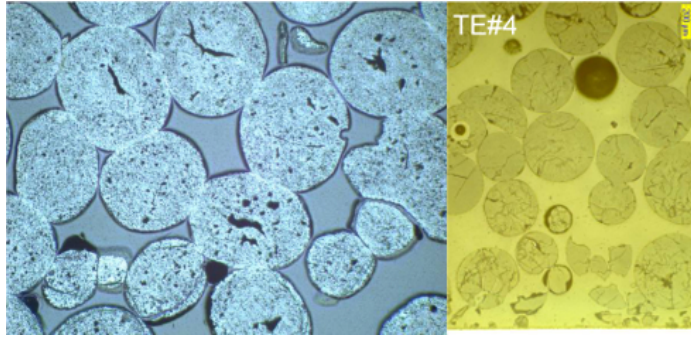


Figure 2.12: Notable features of irradiated  $\text{Li}_2\text{TiO}_3$  and  $\text{Li}_4\text{SiO}_4$  pebble beds from PBAcitemagelsen2011. (Left) Demonstration of significant sintering of  $\text{Li}_2\text{TiO}_3$  pebbles with no fracturing; the visible cracks originated from production and handling. (Right) Demonstration of cracking of  $\text{Li}_4\text{SiO}_4$  pebbles.

creep-compacted ceramic pebble bed is thus expected to be higher than a standard ceramic pebble bed. This phenomenon results in lower temperature gradients and a lower overall temperature magnitude, which is precisely what was observed in the experiment over the course of the cycling.

During PIE, various microscopy preparation techniques are used to study the deformation state of the pebble beds (signs of creep compaction and sintering), formation of gas gaps between the pebble beds and structural materials, and the interaction layers between eurofer-ceramic and eurofer-beryllium.

Figure 2.12 shows the cross-section of  $\text{Li}_2\text{TiO}_3$  pebbles (left) and  $\text{Li}_4\text{SiO}_4$  pebbles (right) post irradiation. Evident in the images is sintering of the lithium titanite and significant fracturing of the lithium orthosilicate pebbles. Importantly, however, it must be noted that the pebble beds performed reliably in spite of the changes displayed in these images citemagelsen2011.

#### 2.4.2 Continuum Modeling of Granular Material for Solid Breeders

When we consider beds of granular material from the standpoint of engineering continuum mechanics, packed beds cannot be adequately described by traditional models of either solids

or liquids alone. Under compression, a packed bed responds like a solid with non-linear elasticity and a plasticity that is history-dependent. At the same time, the packed bed can obviously not support any tensile pressure and will often behave as an extremely viscous liquid as it may fill in voids under just the force of gravity. Nevertheless, phenomenological models, derived from the volumes of collected data, have been developed, using effective material properties for the ceramic pebble bed, that describe the pebble beds in an Eulerian manner that provide reliable information on the initial states of breeder volumes in the fusion reactor environment and allow reasonable design predictions of the Thermomechanics of the breeding blanket.

In spite of the shortcomings of a continuum approach, it is the only option which currently allows treatment of the pebble beds with standard finite element modeling (FEM) that can be scaled up to the breeder system. To employ FEM, mathematical models written in terms of average quantities and containing effective parameters are used. These models deduce a set of constitutive equations to be implemented in the framework of a finite element code. There are two major variants of phenomenological modeling approaches developed among institutions, including: (1) A non-linear elastic model and a modified Drucker-Prager-Cap theory for plastic strain;<sup>57,62</sup> and (2) A hyper-porous non-linear elastic model and a Gurson model for the plastic model.<sup>39–41</sup> Another approach was taken by Ref. <sup>57</sup> wherein the authors employed two different elasticity laws for the loading and unloading branches. Alongside the development of the modeling techniques, several large scale pebble bed Thermomechanics experiments were conducted. These experiments were intended to reveal the underlined thermomechanical characteristics of ceramic breeder pebble beds, and provide data for benchmarking the developed models. The vast amount of work done on modeling the pebble beds in the FEM framework can be found in literature.<sup>39,39,40,40,40,43,43,43,43,62,62,62,64,66,67</sup> A study was also published in 2012 that summarized, compared, and highlighted features of the models under development at the time.<sup>173</sup>

### 2.4.3 Pebble Bed Modeling Benchmarks

The constitutive equations developed for finite element models were derived from the uniaxial compression experiments, which are not fully representative of fusion operating conditions. A more prototypical experiment should subject a pebble bed to isostatic loading. This could be generated by either an in-pile pebble bed experiment or by making use of differential thermal expansion between a pebble bed and its containing structure. The latter has been attempted with several out-of-pile experiments launched by the HE-FUS 3 facility at ENEA Brasimone. The experiments investigated the thermomechanical behavior of pebble beds within geometry much more representative of current breeder designs. These include the medium-scale mock-up exercises of HELICA (HE-FUS3 Lithium Cassette) and HEXCALIBER (HE-FUS3 Experimental Cassette of Lithium Beryllium Pebble Beds).<sup>38,41</sup> For those experiments, the pebble layers are heated by electric heaters, and temperature and displacement were measured.

#### 2.4.3.1 FZK Benchmarking

FZK has performed validation of their FEM code against the data collected from the HELICA experiment.<sup>63</sup> They have also reported the results of simulations of HEXCALIBER but have, as yet, not directly validated against the collected experimental data.<sup>64</sup>

In the HELICA experiment, the pebble beds experienced six thermal ramps, each applied for an hour, and then the pebble beds were actively cooled with a helium flow. After cooling, the pebble beds were subjected to the another thermal ramp and the process was repeated. DIN reports<sup>38</sup> that the pebble bed temperatures exhibited cyclical behavior. FZK simulated two cycles of the HELICA test and an example of the calculated results and experimental data are shown in Figure 2.13 and Figure 2.14. In Figure 2.13 we see temperature histories at a particular location (100 mm from the first wall) during a loading-unloading cycle. The simulation results follow the temperature increase during the thermal ramps up until the seventh hour, then again follow the experimental data as the test rig is cooled with the helium coolant. Even with the two-dimensional simplification of the model, there is

excellent agreement between calculations and measurements. In Figure 2.14 the displacement calculated by FZK is also in strong agreement with the average of measured displacements for the entire duration of the heating-cooling cycle. Because of the overwhelming amount of computer time necessary for the FZK model to complete a fully three-dimensional and transient simulation, the FZK computations of HELICA and HEXCALIBER are carried out in two dimensions; the helium temperature is chosen at an average value of measured inlet and outlet temperatures.

From FZK's numeric simulation arise several important observations: (i) a three-dimensional analysis would provide more detail, spatial temperature variation of e.g. coolants would likely explain much of the deviation between temperature profiles predicted by the simulation and measured in the HELICA experiment; (ii) gap formations, with sizes on the order of a pebble diameter, were detected at the interface of the first wall in ceramic beds; (iii) the maximum hydrostatic pressures seen in the ceramic bed are anticipated to be above the fracturing limit of the lithium ceramic. The consequences of some of these observations, if true and real, are severe enough that they merit careful attention. Gap formation and pebble failure (crush or fracturing) are important topics that must be considered in validation with future experiments.

#### 2.4.3.2 DIN Benchmarking

Because of the characteristics of the DIN model, full three-dimensional simulations were capable of being relatively easily performed. In the framework of benchmarking efforts, DIN has performed validation of their model against experimental results of HELICA, shown in Figure 2.15 as well as HEXCALIBER, shown in Figure 2.16.

The results of the DIN model show also strong agreement to the experimental results of HELICA as demonstrated in one example of temperature histories shown in Figure 2.15. In this profile, the same location as that modeled by FZK (100 mm from the first wall) is simulated by DIN. The FEM simulations from DIN (Figure 2.15) are reported over the six-hour heating portion of a single heating ramp cycle of HELICA. When comparing the

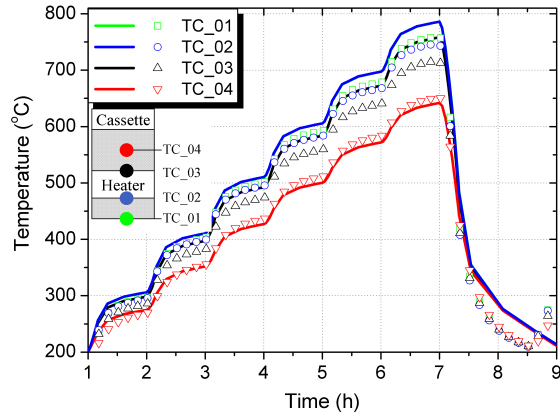


Figure 2.13: Results of the FZK benchmarking with HELICA<sup>64</sup> showing temperature variations with time during a loading cycle ( $T$  in  $^{\circ}\text{C}$ ) at 100 mm from FW.

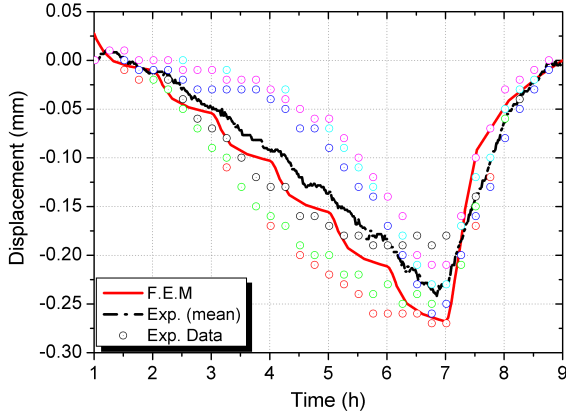


Figure 2.14: Results of the FZK benchmarking with HELICA<sup>64</sup> showing a comparison of displacements (in mm) in HELICA between calculated and measured LVDT values.

results from DIN with those of FZK (in Figure 2.13 and Figure 2.14) we see the DIN model has slightly better predictive capabilities for the temperature histories. This may be due attributed to the three-dimensional variations in coolant temperature being captured by the DIN model.

Unfortunately, the ambitions of HEXCALIBER were limited due to the crippling of several heaters. Nevertheless, the limited data was still used in efforts to validate the constitutive relationships of the DIN model. The temperature variations with time were the only

major result reported by the ENEA Brasimone team, such as that shown in Figure 2.16; mechanical results are still forthcoming from the research group. From the comparisons to experimental measurements in HELICA and HEXCALIBER it is encouraging to notice that even in the absence of a creep model, satisfactorily close agreement were seen between computation and measurement. So far, no detailed displacement comparisons have been made to experimental data.

Several important observations are also made from the results of the DIN simulation: (i) three-dimensional effects were important to calculations of the convective energy transport of the helium coolant; future models should continue to be analyzed in three-dimensions; (ii) DIN reports that in HELICA all ceramic beds experience a compressive force everywhere and no gap formation is ever detected.

In summary, the benchmarking efforts have only recently begun in Europe. A typical pebble bed Thermomechanics simulation involves first calculating overall temperature fields of the blanket unit as it undergoes volumetric nuclear heating as well as cooling at the boundaries. The non-linear mechanical analysis is then performed for stress and strain estimations. However, since the effective thermal conductivity of the ceramic breeder pebble bed is, to some degree, dependent on strain, a coupled thermal and mechanical analysis is needed. Additional details on modeling steps can be found in Refs.<sup>38,39,41,43,64,66</sup> The two most developed models, from FZK and DIN, have had their results compared to experimental data and have thus far shown great promise.

However, it must be noted that the benchmarking efforts are incomplete and inconsistencies between the two models must be explained as they move forward. For example, the model of FZK concluded that a gap appeared between the pebble bed and structural wall, however the model from DIN reported no gap formation. The existence of a gap between pebble bed and structural wall will negatively affect the ability to cool the pebble bed and thereby impact structural and tritium release properties of the bed. That such a discrepancy exists between calculated results of the models on such a critical feature warrants either more benchmarking efforts or a careful deconstruction of the constitutive equations to discover the source of the inconsistency. Future experiments aimed at benchmarking ought to focus on

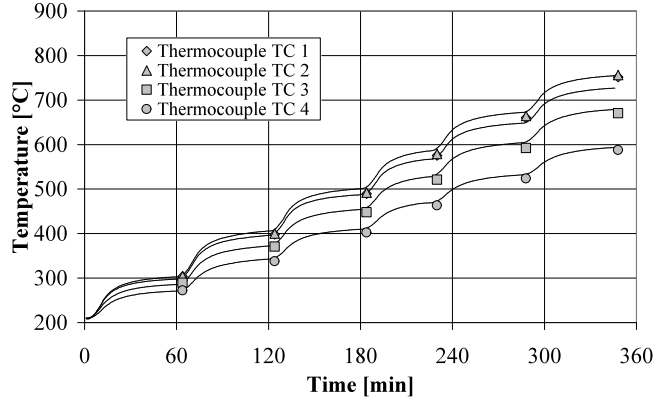


Figure 2.15: Exemplary results of the DIN benchmarking with HELICA: Temperature variations with time during a loading cycle at 100 mm from FW.<sup>40</sup>

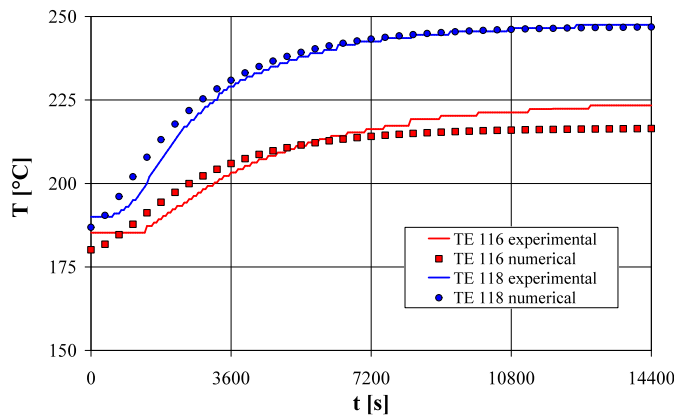


Figure 2.16: Exemplary results of the DIN benchmarking with HEXCALIBER : Temperature variations with time during a loading cycle within the first lithium-orthosilicate cell.<sup>39</sup>

creating apparatus capable of expressing, among other things, when gap formation or pebble failure occurs.

#### 2.4.4 Discrete Element Method for Solid Breeders of Tritium

However, current continuum models will be shown to be insufficient for capturing the evolving thermomechanics of the packed bed as bed resettling, individual grain crushing, and the helium purge influence the packing structure and inter-particle force networks in the bed.

Thus in this dissertation I will approach the pebble bed from the microscopic scale of individual grains via the discrete element method to enable predictive capabilities for temperature profiles in ceramic breeder pebble beds with a helium purge gas – even those experiencing bed resettling and grain crushing. Along the way, new constitutive relationships for material properties are discovered, fragmentation models are created, and new heat transfer models are incorporated.

Correlations for effective properties of heat transfer and the constitutive equations derived from experiments are, however, still incapable of accurate modeling of granular thermomechanics as the granular material evolves in time (based on creep, granular crushing, sintering, *etc.*), thus many researchers of ceramic pebble beds began modeling with the grain-scale discrete element method (DEM). The last part of this chapter revolves around discussion of historical efforts of applying DEM to solid breeders and important results obtained.

A thorough review of the physics behind DEM will be given in ???. For now, we will simply discuss some major results of the implementation of DEM in past solid breeder research.

The Discrete Element Method (DEM) introduced by<sup>34</sup> has been shown to be a promising tool to study the behavior of granular systems through the interaction between the individual particles. DEM was first applied to study the micro-mechanical aspects of cyclic thermal loads on the relaxation of stress in pebble beds for fusion reactors.<sup>105,174</sup> An iterative relaxation strategy of DEM was used to study the internal contact forces in a pebble bed under an external load by An *et al.*<sup>61</sup> The same DEM tools, and the insight provided by which, were also used to initiate DEM-based investigations of creep between pebbles under thermal and mechanical loads.<sup>5</sup> While An *et al.* studied the pebble assemblies in rectangular and cylindrical containers bounded by a elastic walls, computational requirements prevented more than a few thousand particles in the ensemble with rigid walls.<sup>61</sup> Following An's work, the DEM torch was passed across the pond to researchers at KIT where they began to improve upon the initial studies begun at UCLA.

The effect of packing factor, geometry of the assembly on the overall stress-strain response under uniaxial compression tests (UCT) has been thoroughly investigated.<sup>65</sup> Gan

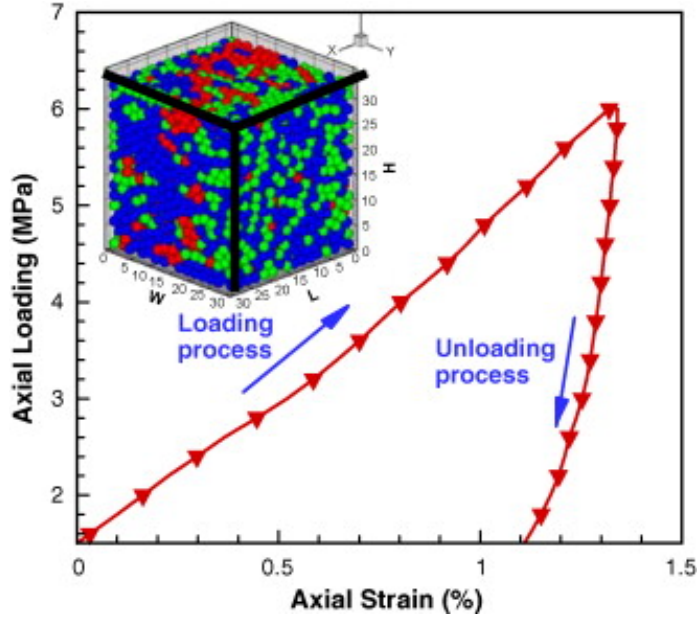


Figure 2.17: Stress–strain behaviors of granular materials in a rectangular box under uniaxial compaction from DEM are qualitatively matched to behaviors seen experimentally.

*et al.* pebble assemblies in a cubic box with periodic boundary conditions to prevent the influence of boundaries dominating the ensemble response to loads.<sup>71</sup> In the DEM uniaxial compression studies (see Figure 2.17), a non-linear stress-strain response and a characteristic residual strain after unloading (analogous to plastic strain in continuum systems) is observed akin to the experimental results.<sup>126</sup> It was shown that the average coordination number, average normal contact force and the maximum normal contact force in the assembly has a unique functional relation (nonlinear, linear and linear, respectively) with the hydrostatic pressure or the applied pressure independent of the packing factor.<sup>5,65</sup> These functional relations may be used as master curves for the micro-macro correspondence in the pebble bed Thermomechanics studies.

Recently, the effect of the pebble size distribution on the overall thermomechanical behavior of the pebble assembly is studied by Annabattula *et al.*<sup>7</sup> They consider the pebble size distribution of ceramic breeder pebbles ( $\text{Li}_4\text{SiO}_4$ ) with a diameter range of 0.25 mm–0.65 mm. Figure 2.18 shows a binary pebble assembly in a periodic box. The colors indicate stored elastic strain energy of the pebble (red: maximum and blue: zero). The assembly has

a maximum pebble radius  $r_g = 0.25$  mm with the pebble size ratio  $r^* = r_s/r_g = 0.6$ , relative volume fraction  $V^* = V_g/V = 0.7$  and a packing factor  $\eta = 0.643$ . The average stress in a granular assembly can be deduced from the contact forces between individual grains.

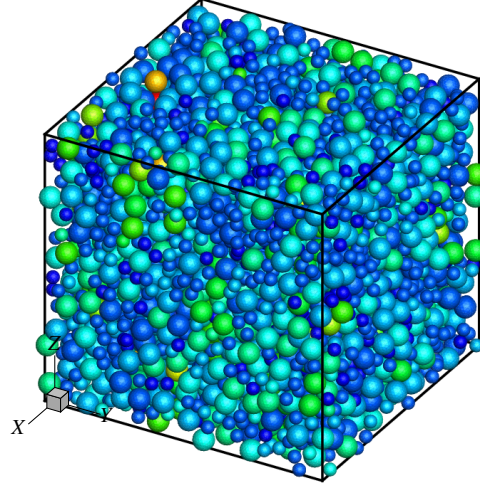


Figure 2.18: A binary pebble assembly with  $r^* = 0.6$  and  $V^* = 0.7$  showing the stored elastic energy of the pebbles at  $\epsilon_{33} = 1.5\%$ ; pebbles of radius  $r_s$  (small) and  $r_g$  (large).

Another aspect of interest in the study of mechanics of pebble beds is the crush behavior of individual pebbles and their impact on the over all pebble bed response. DEM was used to study the behavior of a crushable pebble assembly with the crush load data for  $\text{Li}_4\text{SiO}_4$  pebbles (for individual pebbles) measured at KIT for pebbles of diameter 0.5 mm.

A probabilistic method for analyzing the crush events of individual pebbles and a procedure with the combination of DEM and experimental data to obtain crush load probability has been reported by.<sup>67</sup> Figure 2.19 shows the cumulative distribution function as a function of the hydrostatic pressure placed on the bed. The probability analysis, derived from DEM calculations, provides quantitative report of pebble crushing as a function of a specific hydrostatic pressure. The results of this analysis exemplify the growing strength of DEM techniques for analyses connecting global pebble bed loads to individual pebbles.

However, it has been shown<sup>182, 185</sup> that a criterion based on critical stored elastic energy is the most suitable criterion for describing the  $\text{Li}_4\text{SiO}_4$  pebble failure. Hence, the crush load

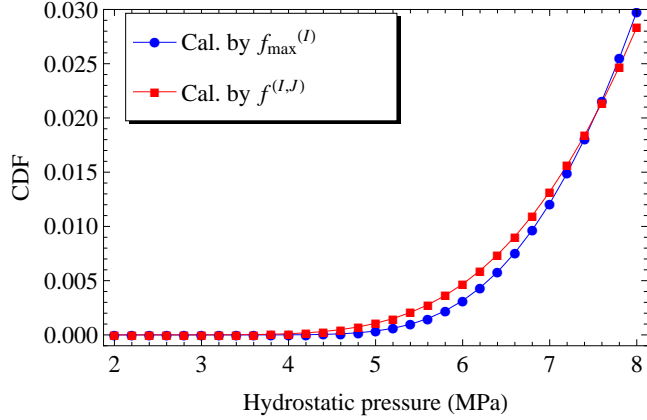


Figure 2.19: Cumulative distribution functions for crushing of individual pebbles inside the bed for as-fabricated pebbles, calculated by (1) maximum contact forces and (2) all inter-particle contact forces.<sup>67</sup>

data (provided by fusion materials laboratory at KIT) has been transformed into equivalent elastic strain energy showing a Weibull distribution.<sup>182</sup> This critical energy (randomly generated distribution) is used as the criterion for failure of pebbles in the DEM simulations. First, the assembly is loaded up to 3% strain in uniaxial compression and then unloaded to a stress-free state. The elastic modulus of the pebble is reduced (from initial value to a small value of 1 kPa) with increase in elastic strain energy of the pebble according to a phenomenological damage accumulation law citeAnnabattula2011b. The damage state is frozen at the end of loading step and hence there will be no further damage accumulation in the unloading step.

Figure. 2.20 shows the results for two types of damage law each with three different realizations. Each realization corresponds to a different random distribution of critical energies assigned to the pebbles in the assembly. The results do not show appreciable sensitivity to random distribution of energies. In the case of gradual damage law, the reduction of the elastic modulus of the pebble starts when the stored elastic energy reaches 50% of the critical energy for that pebble and the elastic modulus reaches exponentially to its minimum value when the stored elastic energy reaches the critical energy prescribed. In the case of sudden damage this reduction starts at a much later stage when the stored elastic energy

reaches 95% of the critical energy of the pebble. Clearly, the assembly with a sudden damage accumulation shows a higher maximum strength compared to the gradual damage. In the case of the gradual damage, the pebbles start to degrade much earlier (at small strain) than in the case of sudden damage. Hence the critical number of pebbles to fail for the onset of maximum strength is reached earlier (at small strain) in gradual damage. It turns out that a mere 0.2% pebbles is the critical number for the onset of maximum strength (stress plateau) observed.

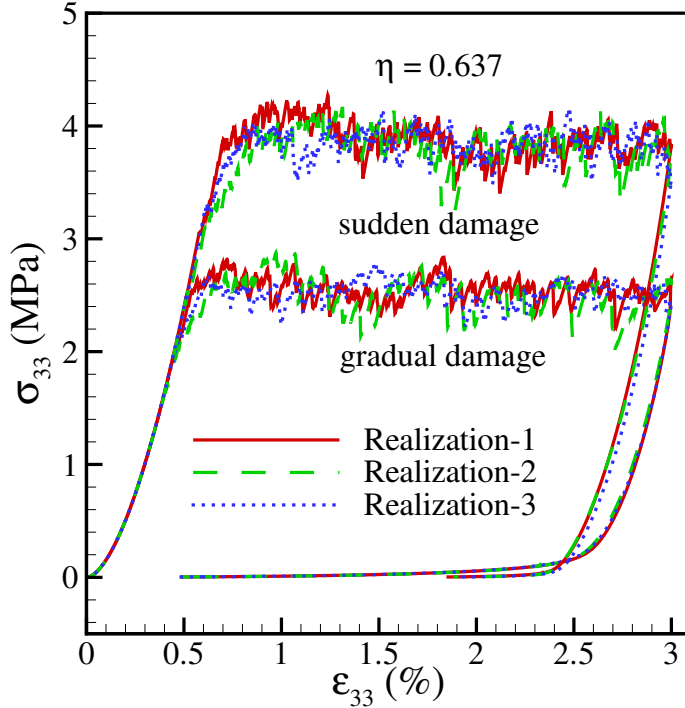


Figure 2.20: Stress-Strain response of a granular assembly under uniaxial compression for two different damage evolution laws (gradual and sudden). Each damage evolution criterion is simulated with three different realizations of randomly prescribed critical failure energy for individual pebbles following Weibull distribution.

The nature of damage evolution influences the maximum strength and strain at which the maximum strength is attained while the critical number of failed pebbles for this saturation is independent of the damage evolution law (also see<sup>182</sup>). Also note that the high frequency oscillations during loading in the stress-plateau region represent the failure of new pebbles. The current analysis also shows a creep-like behavior of the stress-strain response

and hence the stress-plateaus observed in the experiments<sup>126</sup> may indicate the presence of pebble crushing in addition to the thermal creep mechanism. Furthermore, the residual strain after unloading is large for the system with sudden damage than the system with gradual damage. It should be noted that the assembly with gradual damage has more number of damaged pebbles at the end of loading (at 3% strain) making the assembly more compliant than in the case of sudden damage.

#### **2.4.5 Conclusions on Solid Breeder Granular Material Literature Review**

A good deal of progress has been made in the field of ceramic pebble bed analysis. Owing to the multi-scale nature of pebble beds, it is unavoidable that multi-scale models are necessary. In this framework, the continuum modeling approach using FEM and empirically derived material constitutive equations is capable of correctly characterizing the stress load to which a breeder pebble bed unit may be subject during reactor operation. The DEM approach analyzes this load and determines the possibility of pebble bed morphological changes; i.e. pebble damage based on the crush load data of pebbles, the degree of sintering depending on the local contact stress and temperature fields, and creep relaxation of contacts. It is only with the combined analysis of particle-scale information from DEM and system-scale information from FEM that warrants a high confidence of success to the assembly and design of breeder units in a blanket. Experiments should also be conducted to assess the manner of pebble relocations and packing rearrangement when morphological evolution of the pebble bed occurs. It is important to learn if the breeder unit will continue to function in accord with the original design goals under all complex operating conditions. The ultimate objectives of the pebble bed Thermomechanics are: to delineate a near-equilibrium packing state as the initial state, quantify breeder unit Thermomechanics parameters during operations, understand how these properties evolve as topographical changes happen in the packing, and ensure breeder functions as it is intended to in the fusion operational phase spaces.

Lastly, no predictive tool is possible without solid validation attempts. The benchmark

experiments performed up to now were either too limited in scope or practice. New experiments must be performed that can provide reliable data with which to compare numerical results. Fortunately, a new experimental effort out of KIT has been initiated.<sup>80</sup> The experiment shows great promise at reproducing volumetric heating profiles with substantial data collection efforts. The preliminary results are very promising.

## REFERENCES

- [1] Mohamed A Abdou and CW Maynard. Calculational methods for nuclear heating – part II: Applications to fusion-reactor blankets and shields. *Nuclear Science and Engineering*, 56:381–398, 1975.
- [2] Ali Abou-Sena, Alice Y. Ying, and Mohamed A Abdou. Effective Thermal Conductivity of Lithium Ceramic Pebble Beds for Fusion Blankets: A Review. *Fusion Science and Technology*, 47(4):1094–1100, 2005.
- [3] H. T. Aichlmayr and F. a. Kulacki. On the Effective Thermal Conductivity of Saturated Porous Media. *Heat Transfer: Volume 1*, pages 265–273, 2005.
- [4] Amit Amritkar, Surya Deb, and Danesh Tafti. Efficient parallel CFD-DEM simulations using OpenMP. *Journal of Computational Physics*, 256:501–519, 2014.
- [5] Zhiyong An, Alice Ying, and Mohamed A Abdou. Numerical characterization of thermo-mechanical performance of breeder pebble beds. *Journal of Nuclear Materials*, 367–370:1393–1397, 2007.
- [6] Ratna Kumar Annabattula, Yixiang Gan, and Marc Kamlah. Mechanics of binary and polydisperse spherical pebble assembly. *Fusion Engineering and Design*, pages 2–7, mar 2012.
- [7] Majid Bahrami, M.M. Yovanovich, and J. Richard Culham. Effective thermal conductivity of rough spherical packed beds. *International Journal of Heat and Mass Transfer*, 49(19-20):3691–3701, 2006.
- [8] R Bauer and E U Schlunder. Effective Radial Thermal-Conductivity of Packings in Gas-Flow. 2. Thermal-Conductivity of Packing Fraction without Gas-Flow. *International Chemical Engineering*, 18(2):189–204, 1978.
- [9] Sofiane Benyahia, Madhava Syamlal, and Thomas J. O'Brien. Extension of Hill–Koch–Ladd drag correlation over all ranges of Reynolds number and solids volume fraction. *Powder Technology*, 162(2):166–174, mar 2006.
- [10] G Breitbach and H Barthels. The radiant heat transfer in the high temperature reactor core after failure of the afterheat removal systems. *Nuclear Technology*, 49(3):392–399, 1980.
- [11] L. Bühler and Jörg Reimann. Thermal creep of granular breeder materials in fusion blankets. *Journal of Nuclear Materials*, 307-311:807–810, dec 2002.
- [12] P. Calderoni, Alice Ying, Tomas Sketchley, and Mohamed A Abdou. Experimental study of the interaction of ceramic breeder pebble beds with structural materials under thermo-mechanical loads. *Fusion Engineering and Design*, 81(1-7):607–612, 2006.
- [13] P.C. Carman. Fluid flow through granular beds, 1937.

- [14] P.C. Carman. *Flow of Gas Through Porous Media*. London Butterworths Scientific Publications, 1956.
- [15] Seungyon Cho, Mu-Young Ahn, Duck Hoi Kim, Eun Seok Lee, Sunghwan Yun, Nam Zin Cho, and Ki Jung Jung. Current status of design and analysis of Korean Helium-Cooled Solid Breeder Test Blanket Module. *Fusion Engineering and Design*, 83(7-9):1163–1168, dec 2008.
- [16] F. Cismondi, S. Kecskés, M. Ilic, G. Légrádi, B. Kiss, O. Bitz, B. Dolensky, H. Neuberger, L. V. Boccaccini, and T. Ihli. Design update, thermal and fluid dynamic analyses of the EU-HCPB TBM in vertical arrangement. *Fusion Engineering and Design*, 84:607–612, 2009.
- [17] Peter A Cundall and Otto D L Strack. A discrete numerical model for granular assemblies. *Geotechnique*, 29(1):47–65, 1979.
- [18] J a Currie. Gaseous diffusion in porous media. Part 3 - Wet granular materials. *British Journal of Applied Physics*, 12(6):275–281, 2002.
- [19] R. G. Deissler and J. S. Boegli. An investigation of effective thermal conductivities of powders in various gases. *ASME Transactions*, 80(7):1417–1425, 1958.
- [20] G. Dell'Orco, Francesco Paolo Di Maio, R. Giannusso, A Malavasi, L. Sansone, A. Tincani, and G. Vella. Progress in the benchmark exercise for analyzing the lithiate breeder pebble bed thermo-mechanical behaviour. *Fusion Engineering and Design*, 81(1-7):169–174, feb 2006.
- [21] G. Dell'Orco, Francesco Paolo Di Maio, R. Giannusso, A. Tincani, and G. Vella. On the theoretical-numerical study of the HEXCALIBER mock-up thermo-mechanical behaviour. *Fusion Engineering and Design*, 85(5):694–706, aug 2010.
- [22] G. Dell'Orco, P Dimaio, R. Giannusso, A. Tincani, G. Vella, and Francesco Paolo Di Maio. A constitutive model for the thermo-mechanical behaviour of fusion-relevant pebble beds and its application to the simulation of HELICA mock-up experimental results. *Fusion Engineering and Design*, 82(15-24):2366–2374, oct 2007.
- [23] Francesco Paolo Di Maio, G. Dell'Orco, R. Giannusso, A Malavasi, I. Ricapito, A. Tincani, and G. Vella. Experimental tests and thermo-mechanical analyses on the HEXCALIBER mock-up. *Fusion Engineering and Design*, 83(7-9):1287–1293, dec 2008.
- [24] Francesco Paolo Di Maio, Alberto Di Renzo, and Daniela Trevisan. Comparison of heat transfer models in DEM-CFD simulations of fluidized beds with an immersed probe. *Powder Technology*, 193(3):257–265, aug 2009.
- [25] Francesco Paolo Di Maio, R. Giannusso, and G. Vella. On the hyperporous non-linear elasticity model for fusion-relevant pebble beds. *Fusion Engineering and Design*, 85(7-9):1234–1244, 2010.

- [26] Jacques Duran. *Sands, powders, and grains: an introduction to the physics of granular materials*. Springer Science & Business Media, 2012.
- [27] Sabri Ergun. Fluid flow through packed columns. *Chemical engineering progress*, 48, 1952.
- [28] G. Federici, A René Raffray, and Mohamed A Abdou. MISTRAL: A comprehensive model for tritium transport in lithium-based ceramics. Part II: Comparison of model predictions with experimental results. *Journal of Nuclear Materials*, 173:185–213, 1990.
- [29] Y.T. Feng and K. Han. An accurate evaluation of geometric view factors for modelling radiative heat transfer in randomly packed beds of equally sized spheres. *International Journal of Heat and Mass Transfer*, 55(23-24):6374–6383, nov 2012.
- [30] Scott Flueckiger, Zhen Yang, and Suresh V. Garimella. An integrated thermal and mechanical investigation of molten-salt thermocline energy storage. *Applied Energy*, 88(6):2098–2105, jun 2011.
- [31] Scott M. Flueckiger, Brian D. Iverson, Suresh V. Garimella, and James E. Pacheco. System-level simulation of a solar power tower plant with thermocline thermal energy storage. *Applied Energy*, 113:86–96, jan 2014.
- [32] Scott M. Flueckiger, Zhen Yang, and Suresh V. Garimella. Thermocline Energy Storage in the Solar One Power Plant: An Experimentally Validated Thermomechanical Investigation. In *ASME 2011 5th International Conference on Energy Sustainability, Parts A, B, and C*, pages 775–781. ASME, 2011.
- [33] J H Fokkens. Thermo-mechanical Finite Element Analyses for the HCPB In-pile Test Element, 2003.
- [34] F. Franzia, L. V. Boccaccini, a. Ciampichetti, and M. Zucchetti. *Tritium transport analysis in HCPB DEMO blanket with the FUS-TPC code*, volume 88. 2013.
- [35] Yixiang Gan. Thermal Discrete Element Analysis of EU Solid Breeder Blanket Subjected to Neutron Irradiation. *Fusion Science & Technology*, 66, 2014.
- [36] Yixiang Gan and Marc Kamlah. Identification of material parameters of a thermo-mechanical model for pebble beds in fusion blankets. *Fusion Engineering and Design*, 82(2):189–206, feb 2007.
- [37] Yixiang Gan and Marc Kamlah. Thermo-mechanical analysis of pebble beds in HELICA mock-up experiments. *Fusion Engineering and Design*, 83(7-9):1313–1316, dec 2008.
- [38] Yixiang Gan and Marc Kamlah. Thermo-mechanical analyses of HELICA and HEX-CALIBER mock-ups. *Journal of Nuclear Materials*, 386-388:1060–1064, apr 2009.
- [39] Yixiang Gan and Marc Kamlah. Discrete element modelling of pebble beds: With application to uniaxial compression tests of ceramic breeder pebble beds. *Journal of the Mechanics and Physics of Solids*, 58(2):129–144, feb 2010.

- [40] Yixiang Gan and Marc Kamlah. Thermo-mechanical modelling of pebble bed-wall interfaces. *Fusion Engineering and Design*, 85(1):24–32, jan 2010.
- [41] Yixiang Gan, Marc Kamlah, Heinz Riesch-Oppermann, Rolf Rolli, and Ping Liu. Crush probability analysis of ceramic breeder pebble beds under mechanical stresses. *Journal of Nuclear Materials*, pages 10–13, dec 2010.
- [42] F. a. Gilabert, J. N. Roux, and a. Castellanos. Computer simulation of model cohesive powders: Influence of assembling procedure and contact laws on low consolidation states. *Physical Review E - Statistical, Nonlinear, and Soft Matter Physics*, 75:1–26, 2007.
- [43] V Gnielinski. Berechnung des Wärme-und Stoffaustauschs in durchströmten ruhenden Schüttungen. *Verfahrenstechnik*, 16(1):36–39, 1982.
- [44] Klemens Gruber. *Sediment transport in open channel flows - Experimental investigation and numerical simulation of local scour development downstream of a weir*. PhD thesis, 2012.
- [45] D.J. Gunn. Transfer of heat or mass to particles in fixed and fluidised beds. *International Journal of Heat and Mass Transfer*, 21(4):467–476, apr 1978.
- [46] F. Hernández, M. Kolb, Ratna Kumar Annabattula, and a. V.d. Weth. Construction of PREMUX and preliminary experimental results, as preparation for the HCPB breeder unit mock-up testing. *Fusion Engineering and Design*, 89(7-8):1257–1262, 2014.
- [47] F. Hernández, M. Kolb, M. Ilić, a. Kunze, J. Németh, and a. Von Der Weth. Set-up of a pre-test mock-up experiment in preparation for the HCPB Breeder Unit mock-up experimental campaign. *Fusion Engineering and Design*, 88(9-10):2378–2383, 2013.
- [48] James M Hill and A.P.S. Selvadurai. *Mathematics and Mechanics of Granular Materials*. Springer, 2005.
- [49] Reghan J. Hill, Donald L. Koch, and Anthony J. C. Ladd. Moderate-Reynolds-number flows in ordered and random arrays of spheres. *Journal of Fluid Mechanics*, 448:243–278, nov 2001.
- [50] Reghan J. Hill, Donald L. Koch, and Anthony J. C. Ladd. The first effects of fluid inertia on flows in ordered and random arrays of spheres. *Journal of Fluid Mechanics*, 448:213–241, nov 2001.
- [51] Heinrich M. Jaeger, Sidney R. Nagel, and Robert P. Behringer. The Physics of Granular Materials. *Physics Today*, 49(4), 1996.
- [52] Hm Jaeger, Sr Nagel, and Rp Behringer. Granular solids, liquids, and gases. *Reviews of Modern Physics*, 68(4):1259–1273, 1996.
- [53] Christoph Kloss, Christoph Goniva, Alice Hager, Stefan Amberger, and Stefan Pirker. Models, algorithms and validation for opensource DEM and CFD-DEM. *Progress in Computational Fluid Dynamics*, 12(2/3):140–152, 2012.

- [54] Donald L Koch and Reghan J. Hill. Inertial Effects in Suspension and Porous-Media Flows. *Annual Review of Fluid Mechanics*, 33(1):619–647, jan 2001.
- [55] Jintang Li, David J. Mason, and Arun S. Mujumdar. A Numerical Study of Heat Transfer Mechanisms in Gas–Solids Flows Through Pipes Using a Coupled CFD and DEM Model. *Drying Technology*, 21(9):1839–1866, dec 2003.
- [56] Jintang Li and D.J. Mason. A computational investigation of transient heat transfer in pneumatic transport of granular particles. *Powder Technology*, 112(3):273–282, oct 2000.
- [57] Zi Lu, Alice Y Ying, and Mohamed A Abdou. Numerical and experimental prediction of the thermomechanical performance of pebble beds for solid breeder blanket. *Fusion Engineering and Design*, 49-50:605–611, 2000.
- [58] A.J. Magielsen, M M W Peeters, J.B.J. Hegeman, M.P. Stijkel, and Jaap G van der Laan. Analysis of the in-pile operation and preliminary results of the post-irradiation dismantling of the pebble bed assemblies, presented at the 8th ISFNT, 2007.
- [59] G Piazza, Jörg Reimann, E Günther, Regina Knitter, N. Roux, and J D Lulewicz. Characterisation of ceramic breeder materials for the helium cooled pebble bed blanket. *Journal of Nuclear Materials*, 307-311(0):811–816, dec 2002.
- [60] Y Poitevin, Lorenzo Boccaccini, M. Zmitko, I Ricapito, J.F. Salavy, E. Diegele, F. Gabriel, E. Magnani, H. Neuberger, R. Lässer, and L. Guerrini. Tritium breeder blankets design and technologies in Europe: Development status of ITER Test Blanket Modules, test & qualification strategy and roadmap towards DEMO. *Fusion Engineering and Design*, 85(10-12):2340–2347, dec 2010.
- [61] W.E. Ranz and W.R. Marshall. Evaporation From Drops, Part I. *Chemical Engineering Progress*, 48(3):141–146, 1952.
- [62] Jörg Reimann, E. Arbogast, M. Behnke, S. Müller, and K. Thomauske. Thermomechanical behaviour of ceramic breeder and beryllium pebble beds. *Fusion Engineering and Design*, 49-50:643–649, 2000.
- [63] Jörg Reimann, Lorenzo Boccaccini, Mikio Enoda, and Alice Ying. Thermomechanics of solid breeder and Be pebble bed materials. *Fusion Engineering and Design*, 61-62:319–331, nov 2002.
- [64] Jörg Reimann, D. Ericher, and G. Wörner. Influence of pebble bed dimensions and filling factor on mechanical pebble bed properties. *Fusion Engineering and Design*, 69(1-4):241–244, 2003.
- [65] Jörg Reimann and H. Harsch. Thermal creep of beryllium pebble beds. *Fusion Engineering and Design*, 75-79:1043–1047, nov 2005.
- [66] Jörg Reimann and S Hermsmeyer. Thermal conductivity of compressed ceramic breeder pebble beds. *Fusion Engineering and Design*, 61-62:345–351, nov 2002.

- [67] Jörg Reimann and G. Wörner. Thermal creep of Li<sub>4</sub>SiO<sub>4</sub> pebble beds. *Fusion Engineering and Design*, 58-59:647–651, nov 2001.
- [68] Iaea Report. Heat Transport and Afterheat Removal for Gas Cooled Reactors Under Accident Conditions. *Technical Report, IAEA-TECDOC-1163*, 1163, 2000.
- [69] Stefan Rickelt, Florian Sudbrock, Siegmar Wirtz, and Viktor Scherer. Coupled DEM/CFD simulation of heat transfer in a generic grate system agitated by bars. *Powder Technology*, 249:360–372, 2013.
- [70] S J P Romkes, F M Dautzenberg, C M Van Den Bleek, and H P A Calis. CFD modelling and experimental validation of particle-to-fluid mass and heat transfer in a packed bed at very low channel to particle diameter ratio. *Chemical Engineering Journal*, 96:3–13, 2003.
- [71] Oxana Sadovskaya, Vladimir Sadovskii, and Holm Altenbach. *Mathematical Modeling in Mechanics of Granular Materials*. 2012.
- [72] S Song and M Yovanovich. Relative contact pressure-Dependence on surface roughness and Vickers microhardness. *Journal of thermophysics and heat transfer*, 2(1):43–47, 1988.
- [73] Thanit Swasdisevi, Wiwut Tanthapanichakoon, Tawatchai Charinpanitkul, Toshihiro Kawaguchi, Toshitsugu Tanaka, and Yutaka Tsuji. Prediction of gas-particle dynamics and heat transfer in a two-dimensional spouted bed. *Advanced Powder Technology*, 16(3):275–293, jun 2005.
- [74] Hisashi Tanigawa, Mikio Enoeda, and Masato Akiba. Measurement of thermal expansion of Li<sub>2</sub>TiO<sub>3</sub> pebble beds. *Fusion Engineering and Design*, 82(15-24):2259–2263, oct 2007.
- [75] Hisashi Tanigawa, Yuichiro Tanaka, and Mikio Enoeda. Packing behaviour of a Li<sub>2</sub>TiO<sub>3</sub> pebble bed under cyclic loads. *Journal of Nuclear Materials*, 417(1-3):2010–2012, dec 2010.
- [76] W. van Antwerpen, C.G. du Toit, and P.G. Rousseau. A review of correlations to model the packing structure and effective thermal conductivity in packed beds of mono-sized spherical particles. *Nuclear Engineering and Design*, 240(7):1803–1818, jul 2010.
- [77] Jaap G van der Laan, Alexander Fedorov, Sander van Til, and Jörg Reimann. Ceramic Breeder Materials. Technical report, 2011.
- [78] Coert Johannes Visser. *Modelling Heat And Mass Flow Through Packed Pebble Beds: A Heterogeneous Volume-Averaged Approach*. Masters, University of Pretoria, 2007.
- [79] Noriaki Wakao and T. Funazkri. Effect of fluid dispersion coefficients on particle-to-fluid mass transfer coefficients in packed beds. *Chemical Engineering Science*, 33(10):1375–1384, jan 1978.

- [80] Noriaki Wakao and Seiichir\=o Kagei. *Heat and mass transfer in packed beds*, volume 1. Taylor & Francis, 1982.
- [81] Jin Tao Wu, Yu Qiang Dai, Ze Wu Wang, and Feng Xia Liu. Study on the Heat Transfer in Granular Materials by DEM. *Advanced Materials Research*, 233-235:2949–2954, may 2011.
- [82] Zhen Yang and Suresh V. Garimella. Thermal analysis of solar thermal energy storage in a molten-salt thermocline. *Solar Energy*, In Press,, 2010.
- [83] Alice Ying, Jörg Reimann, Lorenzo Boccaccini, Mikio Enoeda, Marc Kamlah, Regina Knitter, Yixiang Gan, Jaap G van der Laan, Lida Magielsen, Francesco Paolo Di Maio, G. Dell'Orco, Ratna Kumar Annabattula, Jon Thomas Van Lew, Hisashi Tanigawa, and Sander van Til. Status of ceramic breeder pebble bed thermo-mechanics R&D and impact on breeder material mechanical strength. *Fusion Engineering and Design*, 87(7-8):1130–1137, aug 2012.
- [84] Alice Y. Ying, Hulin Huang, and Mohamed A Abdou. Numerical simulation of ceramic breeder pebble bed thermal creep behavior. *Journal of Nuclear Materials*, 307-311:827–831, dec 2002.
- [85] P. Zehner and E. U. Schlünder. Wärmeleitfähigkeit von Schüttungen bei mäßigen Temperaturen. *Chemie Ingenieur Technik - CIT*, 42(14):933–941, jul 1970.
- [86] P. Zehner and E. U. Schlünder. Einfluß der Wärmestrahlung und des Druckes auf den Wärmetransport in nicht durchströmten Schüttungen. *Chemie Ingenieur Technik - CIT*, 44(23):1303–1308, 1972.
- [87] Chunbo Zhang, Alice Ying, and Mohamed Abdou. FEM Modeling of Pebble Bed/Structural Wall Separation. *Fusion Science and Technology*, 68(3):612–617, oct 2015.
- [88] Shuo Zhao. *Multiscale Modeling of Thermomechanical Properties of Ceramic Pebbles*. PhD thesis, Karlsruhe Institute of Technology, 2010.
- [89] Shuo Zhao, Yixiang Gan, Marc Kamlah, Tobias Kennerknecht, and Rolf Rolli. Influence of plate material on the contact strength of Li<sub>4</sub>SiO<sub>4</sub> pebbles in crush tests and evaluation of the contact strength in pebble-pebble contact. *Engineering Fracture Mechanics*, 100:28–37, mar 2013.
- [90] Z.Y. Zhou, A.B. Yu, and P. Zulli. Particle scale study of heat transfer in packed and bubbling fluidized beds. *AIChE Journal*, 55(4):868–884, apr 2009.